NASA TECHNICAL NOTE

NASA TN D-5049

C. 1

NASA TN D-5049

TECH LIBRARY KAFB, NM

0131930

LOAN COPY: RETURN TO
AFWL (WLIL-2)
KIRTLAND AFB, N MEX

FIXED-BASE VISUAL SIMULATION OF PILOT-CONTROLLED DESCENTS OF AN ADVANCED APOLLO SPACECRAFT WITH AN ALL-FLEXIBLE PARAWING

by G. Kimball Miller, Jr., Byron M. Jaquet, and Douglas B. Price

Langley Research Center
Langley Station, Hampton, Va.

NATIONAL AERONAUTICS AND SPACE ADMINISTRATION • WASHINGTON, D. C. • MARCH 1969

TECH LIBRARY KAFB, NM

0131930

FIXED-BASE VISUAL SIMULATION OF PILOT-CONTROLLED DESCENTS OF AN ADVANCED APOLLO SPACECRAFT WITH AN ALL-FLEXIBLE PARAWING

By G. Kimball Miller, Jr., Byron M. Jaquet,
and Douglas B. Price

Langley Research Center
Langley Station, Hampton, Va.

NATIONAL AERONAUTICS AND SPACE ADMINISTRATION

For sale by the Clearinghouse for Federal Scientific and Technical Information
Springfield, Virginia 22151 – CFSTI price $3.00

FIXED-BASE VISUAL SIMULATION OF PILOT-CONTROLLED DESCENTS OF AN ADVANCED APOLLO SPACECRAFT WITH AN ALL-FLEXIBLE PARAWING

By G. Kimball Miller, Jr., Byron M. Jaquet,
and Douglas B. Price
Langley Research Center

SUMMARY

A fixed-base visual simulation study has been conducted to determine the ability of an onboard pilot to control an all-flexible parawing and an advanced Apollo capsule combination to preselected landing sites. The investigation employed a closed-circuit television system in conjunction with an earth-terrain model for image generation and permitted six rigid-body degrees of freedom of the vehicle. The pilot controlled the vehicle through the use of a hand controller which activated simulated constant-rate reels to induce rear keel-line changes for pitch control and differential wing-tip line changes for lateral control. The simulated viewing system provided the pilot with a field of view of 34.6° by 48.3°. The optical axis of the viewing system could be controlled in pitch to permit viewing anywhere between the local vertical and the local horizontal. The pilot's task was to assume command of the vehicle at altitudes up to 18 000 feet (5486.4 meters) and control the vehicle to the center of a specified landing site under the influence of various wind profiles with maximum velocities up to 27 ft/sec (8.2 m/sec).

The results of the investigation showed that the pilots could consistently land within about 1400 feet (426.7 meters) of the center of the desired site regardless of the wind conditions or instrumentation employed. The pilots' performances were only slightly degraded when flying in unknown winds. When the maximum wind velocity was greater than 15 ft/sec (4.6 m/sec), the pilots consistently terminated their flights headed in the general direction of the wind to reduce ground speed, whether the winds were known or unknown.

INTRODUCTION

Descent recovery systems suitable for land landings of advanced Apollo spacecraft must possess a certain amount of glide- or range-modulation capability. The feasibility of the land-landing concept was demonstrated in the ground-controlled Gemini gliding-parachute system and in the man-carrying vehicle described in references 1 and 2,

respectively. One of several candidate descent systems for advanced Apollo spacecraft employs an all-flexible parawing of the type described in reference 3.

At the beginning of the present investigation, it was generally believed that the candidate landing system should be controllable to within 3600 feet (1097.3 meters) of the center of a specified landing site. A ground control system incorporating vehicle tracking and current wind profiles was felt to be necessary to achieve the desired landing point accuracy. In addition, it was believed that the onboard pilot would need a wide-angle viewing system to permit simultaneous viewing of the landing site and the current ground position. Turn rates for the parawing-payload combination up to 25° per second were also considered necessary for the pilot to arrive at the desired landing site.

The present fixed-base simulator study was performed to determine the ability of an onboard pilot to control an all-flexible parawing and advanced Apollo capsule combination from initial altitudes up to 18 000 feet (5486.4 meters) and to attain specified landing sites without the benefit of a ground control station. Also, since the flight speeds of the vehicle under consideration are of the same general magnitude as the wind speeds, determination of the effect of winds on the ability of the pilot to attain the landing sites was desirable. Wind speeds of 0 to 27 ft/sec (8.2 m/sec) from various directions were utilized. Whether certain instruments are beneficial in achieving the desired landing sites was also investigated for the various wind conditions. The investigation employed the 1962 U.S. Standard Atmosphere. The basic wind profile was obtained from the NASA Manned Spacecraft Center and was typical of summer winds in southwest Texas.

Since pilots seated in the Apollo capsule cannot see the ground when the capsule is suspended with the heat shield downward, the simulated vehicle incorporated a viewing system which was controllable in pitch by the pilot and which had a field of view of 34.6° by 48.3°. With the viewing system at its maximum downward position, the pilot had a view from the local vertical upward 34.6°. At its maximum upward position, the center line of the viewing system was along the X body axis. A closed-circuit television system and a terrain model were used for image generation.

Observation of wind-tunnel models and radio-controlled model flights indicated that the parawing-payload combination behaved as a rigid body for small motions. Accordingly, equations of motion permitting six rigid-body degrees of freedom were used to represent the vehicle. The equations of motion were solved in real time by an analog computer complex. The pilot, through a two-axis hand controller, closed the control loop and had direct inputs into the force and moment equations. The inputs from the hand controller actuated simulated constant-rate reels which changed the rear keel-line length for pitch control and the right and left tip lines differentially for lateral control.

SYMBOLS

Measurements for this investigation were made in the U.S. Customary Units but are also given in the International System of Units (SI). (See ref. 4.) Transformation matrices for the assumed axis systems are presented in the appendix.

a_X, a_Y, a_Z accelerations due to aerodynamic forces along X-, Y-, and Z-axes, respectively, feet/second^2 (meters/second^2)

b span of flexible wing when flat, feet (meters)

$$C_l = \frac{\text{Rolling moment about X-axis}}{QSb}$$

$$C_m = \frac{\text{Pitching moment about Y-axis}}{QSb}$$

$$C_n = \frac{\text{Yawing moment about Z-axis}}{QSb}$$

$$C_X = \frac{\text{Force along X-axis}}{QS}$$

$$C_Y = \frac{\text{Force along Y-axis}}{QS}$$

$$C_Z = \frac{\text{Force along Z-axis}}{QS}$$

$C_{m,0}$ value of C_m at zero angle of attack

$C_{X,0}$ value of C_X at zero angle of attack

$C_{Z,0}$ value of C_Z at zero angle of attack

$C_{m_\alpha} = \frac{\partial C_m}{\partial \alpha}$, per radian

$C_{X_\alpha} = \frac{\partial C_X}{\partial \alpha}$, per radian

$$C_{Z_\alpha} = \frac{\partial C_Z}{\partial \alpha}, \text{ per radian}$$

$$C_{l_\beta} = \frac{\partial C_l}{\partial \beta}, \text{ per radian}$$

$$C_{n_\beta} = \frac{\partial C_n}{\partial \beta}, \text{ per radian}$$

$$C_{Y_\beta} = \frac{\partial C_Y}{\partial \beta}, \text{ per radian}$$

$$C_{l_p} = \frac{\partial C_l}{\partial \frac{pb}{2V_R}}, \text{ per radian}$$

$$C_{n_p} = \frac{\partial C_n}{\partial \frac{pb}{2V_R}}, \text{ per radian}$$

$$C_{Y_p} = \frac{\partial C_Y}{\partial \frac{pb}{2V_R}}, \text{ per radian}$$

$$C_{m_q} = \frac{\partial C_m}{\partial \frac{qb}{2V_R}}, \text{ per radian}$$

$$C_{X_q} = \frac{\partial C_X}{\partial \frac{qb}{2V_R}}, \text{ per radian}$$

$$C_{Z_q} = \frac{\partial C_Z}{\partial \frac{qb}{2V_R}}, \text{ per radian}$$

$$C_{l_r} = \frac{\partial C_l}{\partial \frac{rb}{2V_R}}, \text{ per radian}$$

$C_{n_r} = \dfrac{\partial C_n}{\partial \dfrac{rb}{2V_R}}$, per radian

$C_{Y_r} = \dfrac{\partial C_Y}{\partial \dfrac{rb}{2V_R}}$, per radian

$\dfrac{\partial C_X}{\partial \left|\dfrac{\Delta L}{l_k}\right|}, \dfrac{\partial C_Z}{\partial \left|\dfrac{\Delta L}{l_k}\right|}, \dfrac{\partial C_m}{\partial \left|\dfrac{\Delta L}{l_k}\right|}$ variation in C_X, C_Z, and C_m due to differential wing-tip deflection

$\dfrac{\partial C_{Y_\beta}}{\partial \left|\dfrac{\Delta L}{l_k}\right|}, \dfrac{\partial C_{n_\beta}}{\partial \left|\dfrac{\Delta L}{l_k}\right|}, \dfrac{\partial C_{l_\beta}}{\partial \left|\dfrac{\Delta L}{l_k}\right|}$ variation in C_{Y_β}, C_{n_β}, and C_{l_β} due to differential wing-tip deflection

$\dfrac{\partial C_X}{\partial \dfrac{\Delta l}{l_k}}, \dfrac{\partial C_Z}{\partial \dfrac{\Delta l}{l_k}}, \dfrac{\partial C_m}{\partial \dfrac{\Delta l}{l_k}}$ pitch control parameters, change in coefficients due to change in rear keel-line length from nominal

$\dfrac{\partial C_Y}{\partial \dfrac{\Delta L}{l_k}}, \dfrac{\partial C_n}{\partial \dfrac{\Delta L}{l_k}}, \dfrac{\partial C_l}{\partial \dfrac{\Delta L}{l_k}}$ lateral control parameters, change in coefficients due to differential deflection of right and left tip lines from the nominal

F_X, F_Y, F_Z aerodynamic forces along X-, Y-, and Z-axes, respectively, pounds (newtons)

$g_\oplus$ acceleration at surface of earth due to gravitational attraction, 32.2 feet/second^2 (9.814 meters/second^2)

H direction of flight referenced to west, defined as angle between V_{xy} and X_c-axis, degrees

ΔH difference in terminal flight-path direction, defined as difference between heading into wind and actual heading, degrees

h altitude above surface of earth, feet (meters)

I_X, I_Y, I_Z moments of inertia about X-, Y-, and Z-axes, respectively, slug-feet^2 (kilogram-meters^2)

L/D lift-drag ratio

ΔL differential deflection of right and left wing-tip lines from nominal, right roll is obtained by shortening right and lengthening left tip lines (positive ΔL), feet (meters)

l_k wing keel length when flat, feet (meters)

Δl change in rear keel-line length from nominal, nominal length is that for trim at $\alpha = 30^{\circ}$, feet (meters)

M_X, M_Y, M_Z aerodynamic moments about X-, Y-, and Z-axes, respectively, foot-pounds (meter-newtons)

m mass of parawing-payload combination, slugs (kilograms)

p,q,r vehicle angular velocities about X-, Y-, and Z-axes, respectively, radians/second or degrees/second

Q dynamic pressure, pounds/foot^2 (newtons/meter^2)

R, Ψ, Y_i cylindrical coordinate system with origin at center of earth and vector R and angle Ψ in $X_i Z_i$-plane (see fig. 1)

$R_{\oplus}$ radius of earth, 20.9×10^6 feet (6.37×10^6 meters)

S area of wing when flat, feet^2 (meters^2)

t time, seconds

V inertial velocity, feet/second (meters/second)

V_R relative wind velocity, feet/second (meters/second)

V_{xy} velocity in plane parallel to surface of earth (ground speed), feet/second (meters/second)

ΔV_{xy} difference in terminal velocity, defined as difference between terminal velocity and that which could have been obtained by heading into wind, feet/second (meters/second)

X,Y,Z orthogonal reference system with origin at center of gravity of parawing-payload combination, referred to as body axes (see fig. 1)

X_c,Y_c,Z_c moving-reference coordinate system with origin at surface of earth and with Z_c-axis alined with the local vertical and positive inward, X_c-axis positive westward, and Y_c-axis positive northward (see fig. 1)

X_i,Y_i,Z_i fixed-reference coordinate system with origin located at center of earth (see fig. 1)

X_{op},Y_{op},Z_{op} optics coordinate system with origin at center of gravity of vehicle (differs from body axes by angle θ_{op} measured from X-axis in XZ-plane) (see fig. 1)

y displacement along the Y_i-axis, feet (meters)

α angle between relative wind velocity and X-axis in XZ-plane, referred to as angle of attack, degrees

β sideslip angle, degrees

γ flight-path angle, degrees

δ bank angle, degrees

θ_{op} angle of optical axis of auxiliary viewing system in X,Z-plane measured from X-axis, degrees

ρ air density, slugs/foot^3 (kilograms/meter^3)

ψ,θ,ϕ Euler angles of rotation relating body axes and fixed-reference system, radians or degrees (see fig. 2)

$\Omega_{Xi},\Omega_{Yi},\Omega_{Zi}$ wind components along X_i-, Y_i-, and Z_i-axes, respectively, feet/second (meters/second) (see fig. 1)

$| \; |$ absolute value

$[\;]$ square matrix

$\{\;\}$ column matrix

$[\;]^T$ transpose of matrix $[\;]$

$[\;]^{-1}$ inverse of matrix $[\;]$

$\left[\Gamma_{m,n}\right]_{\substack{m=B,C,I,O \\ n=B,C,I,O}}$ matrix which transforms a vector from axis system m to axis system n; B, C, I, and O represent body system, moving-reference system, fixed-reference system, and optics system, respectively

A dot over a symbol indicates a time derivative.

EQUATIONS OF MOTION

The equations of motion employed in the present investigation permitted six rigid-body degrees of freedom of the vehicle. (See appendix and figs. 1 and 2.) The force equations were written with respect to the cylindrical coordinates, and the moment equations were written with respect to the body axes. The fixed-reference frame was located at the center of the earth, which was assumed to be a nonrotating homogeneous sphere. The pilot closed the control loop and had direct input into the force and moment equations.

VEHICLE DESCRIPTION

The simulated configuration consisted of a 45° all-flexible parawing with a one-eighth keel-length nose cut, depicted in figure 3, and an advanced Apollo spacecraft suspended as indicated in figure 4. Apparent mass effects for all-flexible parawings are not yet determined and, hence, were not included.

The simulated all-flexible parawing was geometrically similar to the one described in reference 3, including the number and placement of the risers. The wing loading of the vehicle (parawing-payload combination) was 1.28 lb/ft^2 (61.28 N/m^2). The wing material

was assumed to have a weight of 2.2 oz/yd^2 (0.07 kg/m^2) and the risers to have a weight of 0.7 that of the wing. Some basic characteristics of the wing when flat were

$$l_k = 131.8 \text{ feet } (40.2 \text{ meters})$$

$$b = 186.2 \text{ feet } (56.7 \text{ meters})$$

$$S = 12\ 000 \text{ feet}^2 \ (1114.8 \text{ meters}^2)$$

The moments of inertia of the 15 312-pound (6945.4-kg) vehicle (parawing-payload combination) about the vehicle body axes were

$$I_X = 176\ 637 \text{ slug-ft}^2 \ (239\ 487.5 \text{ kg-m}^2)$$

$$I_Y = 177\ 934 \text{ slug-ft}^2 \ (241\ 245.9 \text{ kg-m}^2)$$

$$I_Z = 17\ 113 \text{ slug-ft}^2 \ (23\ 202.0 \text{ kg-m}^2)$$

During descent with the heat shield down, the astronauts' view through the advanced Apollo windows is upward in the direction of the wing. In order to obtain a view of the surface of the earth, an auxiliary viewing system was included. The viewing system used in the simulation had a field of view of 34.6° by 48.3°. The direction of the optical axis of the viewing system could be controlled by the pilot to any angular position between the X body axis and a point 80° below the X body axis. (See fig. 4.)

Flight control was accomplished through the use of a two-axis hand controller which actuated simulated constant-rate ($0.020 l_k$/sec) reels to deflect the right and left wing-tip lines differentially for lateral control and to deflect the rear keel line for pitch control. (Maximum possible control deflections were $\pm 0.10 l_k$, although they were not used.)

SIMULATION EQUIPMENT

The equipment used in the simulation is depicted in figure 5. The view through the auxiliary viewing device of the simulated landing vehicle was generated by a closed-circuit television system in conjunction with an earth-terrain model. A fixed-base instrumented cockpit, shown in figure 6, was fitted with a television monitor that provided a field of view of 34.6° by 48.3°. A two-axis hand controller with a dead band that was 25 percent of maximum deflection in pitch and roll was located to the right of the pilot's seat. A pitch input activated the rear keel-line reel at a constant rate. Roll inputs activated the right and left wing-tip lines differentially. When the controller was released, the control lines remained at their given position but could be returned to the neutral or trim position by pushing a button on the two-axis controller or by deflecting the stick in the opposite direction until the neutral position was reached.

An optical pickup, similar to that described in reference 5, was used in conjunction with an image orthicon television camera with 875 scan lines to obtain the three rotational degrees of freedom of the vehicle. The three translational degrees of freedom were obtained by mounting the optical pickup and camera combination on a transport system that moved relative to the terrain model in response to the output of the force equations. The earth-terrain model was a 22.0- by 34.9-foot (6.7- by 10.6-meter) translucent back-lighted screen, scaled at 9000:1, and was an adaptation of part of the lunar orbit and landing approach simulator of the Langley Research Center (fig. 7). In order to provide higher resolution than was possible with painted terrain features, a transparent aerial photograph (fig. 8) was mounted on the front of the model. This transparency represented an area approximately 15 000 feet (4572.0 meters) square in southwest Texas. It should be noted that model protection considerations imposed a minimum altitude limit of approximately 500 feet (152.4 meters), at which point an electrical stop was activated.

AERODYNAMIC PARAMETERS

The aerodynamic and control parameters employed in the present investigation are shown in figure 9. All parameters are based on the flat-wing span and area. The data in figures 9(a) and 9(c) were obtained from the static wind-tunnel measurements of an 18-foot (5.49-meter) keel-length model presented in reference 3.

The sideslip and dynamic derivatives in figure 9(b), however, were obtained from forced oscillation tests of a 5-foot (1.52-meter) keel-length model in the Langley full-scale tunnel. The small model was used because of its adaptability to existing test equipment. It should be noted that using the oscillatory test technique yields combination derivatives in which the dot or acceleration terms appear. (For example, see refs. 6 and 7.) Thus the derivatives shown in figure 9(b) are combination derivatives and were obtained from measurements of the force and moment components in phase and out of phase with the model motion. Since measurements of the acceleration derivatives do not exist at present, separation of the combination derivatives was impossible. Reference 7, however, indicates that the aerodynamic effect of the acceleration derivatives for rigid leading-edge conical parawings appears to be negligible in the angle-of-attack range below the stall. Thus, the oscillatory measurements were considered to be entirely due to the derivatives as labeled in figure 9(b).

The aerodynamic data used in this study were generally available at angles of attack of 30° and above in increments of 5°. Data below an angle of attack of 30° could not be measured under dynamic conditions, because the parawing nose tended to collapse. Thus, in some cases the data were extrapolated to obtain values at an angle of attack of 25°. The aerodynamic data were programed on function generators of analog computers in the

straight line segments shown in figure 9. It should be noted that the data indicate the possibility of a pitch-up problem at angles of attack above 40° and an instability problem in yaw due to a sign change in C_{n_r} at angles of attack below about 28°. The variation of the static lateral parameters with differential lateral control deflection was obtained from reference 3.

TASK DESCRIPTION

A map of the seven landing sites used in the investigation is shown in figure 10. These landing sites were to be attained from 10 initial deployment points with altitudes which ranged from 8000 feet (2438.4 meters) to 18 000 feet (5486.4 meters) and inertial velocities of 20 ft/sec (6.1 m/sec) vertically and 40 ft/sec (12.2 m/sec) horizontally. Several wind profiles (fig. 11), scaled in decreasing magnitude from A to F and a zero wind case, were used in the investigation.

Prior to participation in the program, each pilot was given a description of the simulated vehicle, was told the scope of the investigation, and was given a map (fig. 10) of the area showing the various landing sites. The task of the pilot was to control the vehicle to as close to the center of a specified landing site as possible with the vehicle preferably heading into the wind at flight termination (500-foot (152.4-meter) altitude) to reduce the forward speed relative to the ground. The pilots had knowledge of the approximate downrange capability of the vehicle in still air at a given altitude. In some cases, the terminal magnitude and direction of the wind were known by the pilots. In other cases, the pilots had to determine wind conditions by visual observation of the ground. It should be noted that for a given flight, the wind profile was always chosen so that the landing site could be attained with proper maneuvering.

VEHICLE MANEUVERING CAPABILITY

The computed maneuvering capability of the vehicle in still air is shown in figure 12 which presents the results of a digital-program solution of the simulated vehicle. The digital results indicate that the turn rate varies linearly with differential wing-tip deflection up to about 9° per second in steady turns. Turn rates of less than 8° per second were generally preferred by the pilots because of stability and control problems at angles of attack above 40° and below 28° and because of the limited field of view. The stability problems at the indicated angles of attack limited the useful lift-drag ratio L/D to between 1.5 and 1.8. This range afforded little control over vertical velocity which in all cases was between 14 ft/sec (4.3 m/sec) and 18 ft/sec (5.5 m/sec). The minimum steady turn radius used by the pilots was approximately 250 feet (76.2 meters) at a $\Delta L/l_k$ of

0.06. A turn rate of 5° per second permits a 360° turn to be made while decreasing the altitude by approximately 1000 feet (304.8 meters).

The ground track of a simulated flight of the vehicle performing 360° turns at constant rates up to 6.9° per second is presented in figure 13 for a zero wind case and a low wind case (profile F). A comparison of the results presented in figure 12 and the results of the zero wind case presented in figure 13 shows good agreement between the digital and simulation solutions. The low wind profile used in figure 13 has a maximum wind of 2.7 ft/sec (0.82 m/sec) and does not displace the vehicle significantly during a 360° turn.

The data presented herein were obtained by using reel rates of $0.020l_k$/sec. This value was considered desirable on the basis of achieving small and large inputs without overcontrolling. Reel rates below $0.015l_k$/sec resulted in a response which was too slow and values above $0.025l_k$/sec resulted in overshoot problems in which a desired control-line position was difficult to obtain.

RESULTS AND DISCUSSION

Two research pilots and three research engineers acted as pilots during the investigation. Each pilot performed six introductory flights for familiarization purposes before any data were recorded. No significant difference exists between the performances of the various pilots, and in general, no differentiation is made in the presentation of results.

Miss Distances

Of primary concern in this investigation was a determination of the miss distances in attaining the center of the desired landing sites under the influence of various winds. This information is presented in table I, in the form of the arithmetic mean and the standard deviation from the mean of the miss distance from the center of a given landing site for flights performed in low winds, high winds, and winds which were unknown to the pilots.

Low wind conditions, which had maximum velocities of 0 to about 12 ft/sec (3.66 m/sec), resulted from using wind profiles C to F and a zero wind case. High wind conditions A and B had maximum velocities that were greater than 15 ft/sec (4.57 m/sec) but less than 30 ft/sec (9.14 m/sec). Four additional wind cases with maximum velocities less than 30 ft/sec (9.14 m/sec) were used in the unknown wind flights so that the pilots were required to detect winds blowing from any quadrant. Flights performed under the influence of high wind conditions resulted in larger miss distances than flights performed in low winds. When the winds were unknown, the miss distances were generally greater than those for high winds. In all cases, however, the miss distances are small, being generally less than 1400 feet (426.7 meters) as compared with the acceptable miss distance of 3600 feet (1097.3 meters).

TABLE I.- MISS DISTANCES

Wind conditions	Instrumentation	Miss distance				No. of runs
		Arithmetic mean		Standard deviation		
		ft	m	ft	m	
Low	Full	725.1	221.0	427.9	130.4	32
Low	$\frac{\Delta L}{l_k}$ and $\frac{\Delta l}{l_k}$ only	325.4	99.2	291.8	88.9	32
High	Full	770.1	234.7	567.7	173.0	30
High	$\frac{\Delta L}{l_k}$ and $\frac{\Delta l}{l_k}$ only	409.1	124.7	333.3	101.6	22
Unknown	Full	883.7	269.4	512.4	156.2	34
Unknown	$\frac{\Delta L}{l_k}$ and $\frac{\Delta l}{l_k}$ only	552.7	168.5	375.9	114.6	50
All flights		618.6	188.5	446.4	136.1	200

The miss distances for flights made with partial instrumentation $\left(\frac{\Delta L}{l_k} \text{ and } \frac{\Delta l}{l_k} \text{ only}\right)$ are considerably smaller than those experienced with full instrumentation regardless of the wind condition. Two factors contribute to this difference in miss distance. The primary factor is the effect of training on the pilots' performance. The flights made with partial instrumentation were performed late in the study and had uniformly low miss distances, whereas the flights made with all the instruments were performed prior to the partially instrumented flights and had more scattered miss distances. The second factor contributing to the attainment of smaller miss distances with partial instrumentation was that the pilots used somewhat different flight techniques. When full instrumentation was available, the pilots monitored angle of attack rather closely during their terminal maneuvers in order to avoid regions of instability. However, when no instrumentation except control-line position indicators was available, the pilots merely used controls which they knew would not result in operating in regions of instability and concentrated more heavily on observing the desired landing site during terminal maneuvers. This latter effect was noted by comparing the last 10 flights performed with full instrumentation with the last 10 flights performed with partial instrumentation. All these flights were performed at approximately the same time in the study and show a mean distance of 475 feet (144.8 meters) with full instrumentation and 325 feet (99.1 meters) with partial instrumentation.

It should be noted that all miss distances were measured at an altitude of 500 feet (152.4 meters). If the simulation had permitted flight to zero altitude, the resulting improvement in the pilots' ability to judge altitude and velocity should have resulted in smaller terminal miss distances.

Piloting Techniques

Low winds.- Ground tracks of flights made under the influence of several low wind profiles are presented in figures 14 to 16. The pilots generally flew to the vicinity of the landing sites before maneuvering to lose altitude, regardless of the instrumentation available. With the low wind profiles, the pilots generally performed spiraling descents to lose altitude in the vicinity of the landing site, but they occasionally flew to the downwind side of the site and made S-turns into the wind to lose altitude. During a given flight, the pilots generally positioned the controllable viewing system to see the landing site initially and repositioned it downward to keep the site in view as the site was approached.

The ground tracks (figs. 14 to 16) indicate that the maneuvers performed by the pilots did not vary significantly whether they had all the instrumentation available or had only control-line position indicators. Also, time histories of flights performed with full or partial instrumentation do not differ significantly. Figure 17 is typical of either degree of instrumentation.

The terminal velocity in the horizontal plane (ground speed or V_{xy}) and the vehicle flight-path direction at flight termination are presented in figure 18 for several flights. Plain, flagged, and lined symbols indicate that the yaw rate at flight termination was 0 to 1° per second, 1 to 5° per second, or 5 to 9° per second, respectively. The solid curve is based on a vehicle trimmed at an angle of attack of 30° with a velocity in still air of 29.5 ft/sec (9.0 m/sec) and represents the variation of the terminal horizontal velocity with terminal flight-path direction for the various low wind profiles. For the low wind profiles, little reduction in ground speed could be achieved by heading into the wind. Consequently, the pilots generally ignored the low winds and concentrated on flying as close to the landing site as possible. As the wind magnitude increased, the pilots became more selective in their terminal flight-path direction. For wind case C (fig. 18), the pilots began to fly into the wind, and this maneuver resulted in about a 35-percent reduction in ground speed over that experienced in still air.

High winds.- The ground tracks of flights performed under the influence of high winds (figs. 19 and 20) indicate that the pilots generally flew to the downwind side of the landing site, turned into the wind to land, and performed S-turns to lose altitude if they were going to overshoot the center of the landing site. No significant difference between fully instrumented and partially instrumented flights was detected in either the ground tracks or in the time histories of high wind flights. Figure 21 is typical of the time

histories of flights made with either degree of instrumentation. Significant reductions in ground speed V_{xy} can be realized by flying into the wind with high wind profiles (up to 90 percent for the highest wind condition). Consequently, the pilots consistently terminated their flights in directions which gave near-minimum ground speed. (See fig. 22.)

Unknown winds.- A number of flights were made in which the pilots were not given wind information and were required to determine the wind direction from observing their passage over the ground. The ground tracks of five typical flights are presented in figure 23. In all cases, the pilots (research engineers only) initially alined the vehicle with the desired landing site.

When the winds were low, the pilots often could not detect them early in the flight. In these cases, the pilots often flew up to a road or ditch and then turned to fly along the landmark in an attempt to detect a wind component normal to the landmark. The pilots then generally made a 90° turn toward the desired landing site and attempted to detect the wind component normal to their flight path. If these two maneuvers indicated that the winds were low, the pilots flew to the landing site and performed a spiraling descent. This technique was employed in three of the low wind flights presented in figure 23. In some low wind flights, the pilots initially alined their vehicle with the desired landing site and maintained that heading until reaching the vicinity of the site. If the vehicle had not been blown very far off course, the pilots concluded that the winds were low and spiraled in the area of the landing site to descend.

High winds were generally detected early in the flight. The pilots observed that when the vehicle was initially alined with the desired landing site, it was quickly blown off that heading. The pilots generally attempted to fly to the landing site in high winds but let the wind blow them toward the downwind side of the site. They then turned into the wind and flew toward the center of the site. If the vehicle was going to overshoot the center of the landing site, S-turns were performed to lose altitude. In the high wind flight shown in figure 23, the pilot was late in beginning his S-turn maneuver and had to loop back to the downwind side in order to approach the center of the landing site headed into the wind.

The time histories of flights made in unknown winds are typified by those previously presented and are not included. When the winds were unknown, the pilots could determine the approximate wind direction and magnitude sufficiently well by tracking terrain features to head into the wind when high wind profiles were being used. This technique is exemplified in figure 24 in which the terminal flight-path direction and velocity errors for flights made under the influence of a high and a low wind profile are presented. When the pilots felt that the winds were low, they made no particular attempt to terminate the flight headed into the wind.

Pilots' comments.- The research pilots indicated that the simulated flight characteristics, including turn rates, would be satisfactory if they are representative of the

full-scale vehicle. Various reel rates were investigated, the rates below $0.015l_k$/sec resulting in sluggish control and the rates above $0.025l_k$/sec resulting in overshoot. A reel rate of $0.020l_k$/sec was considered the most satisfactory and was used for all data presented herein. A greater usable angle-of-attack range would be desirable, however, so that more L/D control would be available. The heading and altitude indicators were felt to be beneficial. The lateral control-line and pitch-line position indicators were felt to be mandatory in order to avoid inadvertently operating in a region where divergence could occur. Although the small-angle movable field of view was adequate, the research pilots recommended a wide-angle field of view that would permit the simultaneous monitoring of the landing site and the current ground position. In addition, the pilots felt that their performances would be improved if the simulation provided greater depth cues below 2000 feet (609.6 meters) and provided the capability of continuing the simulated flights to ground level.

CONCLUDING REMARKS

A fixed-base visual simulation study has been conducted to determine the ability of an onboard pilot to control an all-flexible parawing and advanced Apollo capsule combination to attain desired landing sites without the benefit of a ground control station. The investigation included all six rigid-body degrees of freedom of the vehicle. The pilots' task was to assume command of the landing vehicle at altitudes up to 18 000 feet (5486.4 meters) and control the vehicle to attain the center of a specified landing site under the influence of both known and unknown winds.

Within the limits of the simulation, the results of the study showed that regardless of the wind conditions or the instrumentation used, the pilots could consistently attain small miss distances with respect to the center of the desired landing sites. Flights performed under the influence of wind profiles with maximum velocities greater than 15 ft/sec (4.6 m/sec) resulted in larger miss distances than flights performed in lower winds. When the winds were unknown and the pilots were required to track surface features to evaluate the winds, the miss distances were somewhat greater than those for high known winds. In all cases, however, the miss distances were generally less than 1400 feet (426.7 meters). When the maximum wind velocity was greater than 15 ft/sec (4.6 m/sec), the pilots consistently terminated their flights headed in the general direction of the wind to reduce ground speed whether the winds were initially known or unknown. When the maximum wind velocity was less than 15 ft/sec (4.6 m/sec), the pilots generally ignored their final heading and concentrated on attaining small miss distances.

For the specific task investigated, the simulated flight characteristics including turn-rate capability were satisfactory, although a larger usable angle-of-attack range and the resulting increased modulation in the lift-drag ratio would be desirable. Heading and

altitude indicators were desirable, and control-line position indicators were felt to be necessary instruments. The small-angle movable field-of-view system used in the simulation was adequate, although a wide-angle field-of-view system may be desirable.

Langley Research Center,
National Aeronautics and Space Administration,
Langley Station, Hampton, Va., December 13, 1968,
125-19-01-22-23.

APPENDIX

COORDINATE SYSTEMS AND EQUATIONS OF MOTION

The equations used in the simulation allowed three translational and three rotational degrees of freedom. The choice of the forms of the equations and the axis systems was based on the requirements of the lunar orbit and landing approach simulator at the Langley Research Center.

Coordinate Systems

The five coordinate systems used are shown in figure 1. They are

(1) Fixed-reference set X_i, Y_i, and Z_i with origin at the center of the earth and axes fixed with respect to the earth.

(2) Cylindrical set R, Ψ, and Y_i with origin at the center of the earth and the vector R and angle Ψ in the X_iZ_i-plane.

(3) Moving-reference set X_c, Y_c, and Z_c with origin lying on the surface of the earth and the X_cZ_c-plane lying in the X_iZ_i-plane. The positive direction of the Z_c-axis is along the vector R toward the center of the earth.

(4) Body set X, Y, and Z with origin at the center of gravity of the combined parawing-payload vehicle and corresponding to the principal axes of the vehicle.

(5) Optics set X_{op}, Y_{op}, and Z_{op} with origin at the center of gravity of the combined vehicle and differing from the body set only by the angle θ_{op} of the optical axis of the viewing system with respect to the body X-axis. The angle θ_{op} is in the XZ-plane and positive in the direction shown in figure 4.

The Euler angles ψ, θ, and ϕ which describe the orientation of the body axes with respect to the fixed-reference axes are shown in figure 2. The matrix which transforms a vector from the fixed-reference system to the body system is given by

$$\left[\Gamma_{I,B}\right] = \begin{bmatrix} a_{11} & a_{12} & a_{13} \\ a_{21} & a_{22} & a_{23} \\ a_{31} & a_{32} & a_{33} \end{bmatrix} \tag{A1}$$

where

$$a_{11} = \cos\theta \cos\psi$$

APPENDIX

$$a_{12} = \cos\theta \sin\psi$$

$$a_{13} = -\sin\theta$$

$$a_{21} = \sin\phi \sin\theta \cos\psi - \cos\phi \sin\psi$$

$$a_{22} = \sin\phi \sin\theta \sin\psi + \cos\phi \cos\psi$$

$$a_{23} = \sin\phi \cos\theta$$

$$a_{31} = \cos\phi \sin\theta \cos\psi + \sin\phi \sin\psi$$

$$a_{32} = \cos\phi \sin\theta \sin\psi - \sin\phi \cos\psi$$

$$a_{33} = \cos\phi \cos\theta$$

The matrix which transforms a vector from the moving-reference axis system to the fixed-reference system is given by

$$\left[\Gamma_{C,I}\right] = \begin{bmatrix} \cos\Psi & 0 & -\sin\Psi \\ 0 & 1 & 0 \\ \sin\Psi & 0 & \cos\Psi \end{bmatrix} \tag{A2}$$

The matrix which transforms a vector from the moving-reference axis system to the body-axis system is given by

$$\left[\Gamma_{C,B}\right] = \left[\Gamma_{I,B}\right]\left[\Gamma_{C,I}\right] \tag{A3}$$

The matrix which transforms a vector from the body-axis system to the optics-axis system is given by

$$\left[\Gamma_{B,O}\right] = \begin{bmatrix} \cos\theta_{op} & 0 & \sin\theta_{op} \\ 0 & 1 & 0 \\ -\sin\theta_{op} & 0 & \cos\theta_{op} \end{bmatrix} \tag{A4}$$

APPENDIX

Since each of the transformation matrices is orthogonal, each has an inverse equal to its transpose; that is,

$$\left[\Gamma_{I,B}\right]^{-1} = \left[\Gamma_{B,I}\right] = \left[\Gamma_{I,B}\right]^{T}$$

Force Equations

The equations of motion for the three translational degrees of freedom are written in the cylindrical-axis system:

$$\ddot{R} - R\dot{\Psi}^2 = \frac{-F_{Zc}}{m} - g_{\oplus}\left(\frac{R_{\oplus}}{R}\right)^2 \tag{A5}$$

$$R\ddot{\Psi} + 2\dot{R}\dot{\Psi} = \frac{F_{Xc}}{m} \tag{A6}$$

$$\ddot{Y}_i = \frac{F_{Yc}}{m} \tag{A7}$$

The second term on the left-hand side of equations (A5) and (A6) was found to be much less than the first term and was, therefore, neglected in the simulation. The symbols F_{Xc}, F_{Yc}, and F_{Zc} are the aerodynamic forces along the X_c-, Y_c-, and Z_c-axes, respectively, and are given by

$$\begin{Bmatrix} F_{Xc} \\ F_{Yc} \\ F_{Zc} \end{Bmatrix} = \left[\Gamma_{C,B}\right]^{T} \begin{Bmatrix} F_X \\ F_Y \\ F_Z \end{Bmatrix} \tag{A8}$$

where

$$F_X = QS\left[C_{X,0} + C_{X_\alpha}\alpha + C_{X_q}\frac{qb}{2V_R} + \frac{\partial C_X}{\partial \frac{\Delta l}{l_k}}\frac{\Delta l}{l_k} + \frac{\partial C_X}{\partial \left|\frac{\Delta L}{l_k}\right|}\left|\frac{\Delta L}{l_k}\right|\right] \tag{A9}$$

$$F_Y = QS\left[C_{Y_\beta}\beta + C_{Y_p}\frac{pb}{2V_R} + C_{Y_r}\frac{rb}{2V_R} + \frac{\partial C_Y}{\partial \frac{\Delta L}{l_k}}\frac{\Delta L}{l_k} + \frac{\partial C_{Y_\beta}}{\partial \left|\frac{\Delta L}{l_k}\right|}\beta\left|\frac{\Delta L}{l_k}\right|\right] \tag{A10}$$

$$F_Z = QS\left[C_{Z,0} + C_{Z_\alpha}\alpha + C_{Z_q}\frac{qb}{2V_R} + \frac{\partial C_Z}{\partial \frac{\Delta l}{l_k}}\frac{\Delta l}{l_k} + \frac{\partial C_Z}{\partial\left|\frac{\Delta L}{l_k}\right|}\left|\frac{\Delta L}{l_k}\right|\right] \tag{A11}$$

Moment Equations

The equations of motion for the three rotational degrees of freedom are written in the body-axis system:

$$\dot{p} = \frac{1}{I_X}\left[M_X + \left(I_Y - I_Z\right)qr\right] \tag{A12}$$

$$\dot{q} = \frac{1}{I_Y}\left[M_Y + \left(I_Z - I_X\right)rp\right] \tag{A13}$$

$$\dot{r} = \frac{1}{I_Z}\left[M_Z + \left(I_X - I_Y\right)pq\right] \tag{A14}$$

The aerodynamic moments are given by

$$M_X = QSb\left[C_{l_\beta}\beta + C_{l_p}\frac{pb}{2V_R} + C_{l_r}\frac{rb}{2V_R} + \frac{\partial C_l}{\partial \frac{\Delta L}{l_k}}\frac{\Delta L}{l_k} + \frac{\partial C_{l_\beta}}{\partial\left|\frac{\Delta L}{l_k}\right|}\beta\left|\frac{\Delta L}{l_k}\right|\right] \tag{A15}$$

$$M_Y = QSb\left[C_{m,0} + C_{m_\alpha}\alpha + C_{m_q}\frac{qb}{2V_R} + \frac{\partial C_m}{\partial \frac{\Delta l}{l_k}}\frac{\Delta l}{l_k} + \frac{\partial C_m}{\partial\left|\frac{\Delta L}{l_k}\right|}\left|\frac{\Delta L}{l_k}\right|\right] \tag{A16}$$

$$M_Z = QSb\left[C_{n_\beta}\beta + C_{n_p}\frac{pb}{2V_R} + C_{n_r}\frac{rb}{2V_R} + \frac{\partial C_n}{\partial \frac{\Delta L}{l_k}}\frac{\Delta L}{l_k} + \frac{\partial C_{n_\beta}}{\partial\left|\frac{\Delta L}{l_k}\right|}\beta\left|\frac{\Delta L}{l_k}\right|\right] \tag{A17}$$

The angles ψ, θ, and ϕ are Euler angles of the body-axis system with respect to the fixed-reference axes. The Euler angle rates are given by

$$\dot{\psi} = \frac{1}{\cos\theta}(q \sin\phi + r \cos\phi) \tag{A18}$$

$$\dot{\theta} = q \cos\phi - r \sin\phi \tag{A19}$$

$$\dot{\phi} = p + \tan\theta(q \sin\phi + r \cos\phi) \tag{A20}$$

The order of rotation is ψ, θ, and ϕ. These equations are integrated to get the Euler angles used in equation (A1).

The angles used to drive the optical pickup are ψ', θ', and ϕ', the Euler angles of the optics-axis system with respect to the moving-reference axis system. The matrix which transforms a vector from the moving-reference axis system to the optics-axis system is given by

$$\left[\Gamma_{C,O}\right] = \begin{bmatrix} \gamma_{11} & \gamma_{12} & \gamma_{13} \\ \gamma_{21} & \gamma_{22} & \gamma_{23} \\ \gamma_{31} & \gamma_{32} & \gamma_{33} \end{bmatrix} = \left[\Gamma_{B,O}\right]\left[\Gamma_{C,B}\right] \tag{A21}$$

where

$$\gamma_{11} = \cos\theta' \cos\psi'$$

$$\gamma_{12} = \cos\theta' \sin\psi'$$

$$\gamma_{13} = -\sin\theta'$$

$$\gamma_{21} = \sin\phi' \sin\theta' \cos\psi' - \cos\phi' \sin\psi'$$

$$\gamma_{22} = \sin\phi' \sin\theta' \sin\psi' + \cos\phi' \cos\psi'$$

$$\gamma_{23} = \sin\phi' \cos\theta'$$

$$\gamma_{31} = \cos\phi' \sin\theta' \cos\psi' + \sin\phi' \sin\psi'$$

$$\gamma_{32} = \cos\phi' \sin\theta' \sin\psi' - \sin\phi' \cos\psi'$$

$$\gamma_{33} = \cos\phi' \cos\theta'$$

Thus, the angles ψ', θ', and ϕ' are given by

$$\left.\begin{aligned} \sin\theta' &= -\gamma_{13} \\ \cos\theta' &= +\sqrt{1 - \left(\gamma_{13}\right)^2} \end{aligned}\right\} \qquad \left(-\frac{\pi}{2} < \theta' < \frac{\pi}{2}\right) \tag{A22}$$

$$\left.\begin{aligned} \sin \phi' &= \frac{\gamma_{23}}{\cos \theta'} \\ \cos \phi' &= \frac{\gamma_{33}}{\cos \theta'} \end{aligned}\right\} \tag{A23}$$

$$\left.\begin{aligned} \sin \psi' &= \frac{\gamma_{12}}{\cos \theta'} \\ \cos \psi' &= \frac{\gamma_{11}}{\cos \theta'} \end{aligned}\right\} \tag{A24}$$

Auxiliary Equations

Dynamic pressure is given by

$$Q = \frac{1}{2}\rho V_R^2 \tag{A25}$$

where

$$V_R = \sqrt{\left(u + \Omega_X\right)^2 + \left(v + \Omega_Y\right)^2 + \left(w + \Omega_Z\right)^2} \tag{A26}$$

and u, v, and w are components of the inertial velocities along the body X-, Y-, and Z-axes, respectively, and Ω_X, Ω_Y, and Ω_Z are the wind components along the X-, Y-, and Z-axes, respectively, with

$$\begin{Bmatrix} \Omega_X \\ \Omega_Y \\ \Omega_Z \end{Bmatrix} = \left[\Gamma_{I,B}\right] \begin{Bmatrix} \Omega_{Xi} \\ \Omega_{Yi} \\ \Omega_{Zi} \end{Bmatrix} \tag{A27}$$

$$\begin{Bmatrix} u \\ v \\ w \end{Bmatrix} = \left[\Gamma_{C,B}\right] \begin{Bmatrix} \dot{X}_c \\ \dot{Y}_c \\ \dot{Z}_c \end{Bmatrix} \tag{A28}$$

and

$$\left.\begin{aligned} \dot{X}_c &= R\dot{\Psi} \\ \dot{Y}_c &= \dot{Y}_i \\ \dot{Z}_c &= -\dot{R} \end{aligned}\right\} \tag{A29}$$

Equations for the angle of attack, sideslip angle, flight-path angle, and altitude are given by

$$\left.\begin{aligned} \sin\alpha &= \frac{w + \Omega_Z}{\sqrt{\left(w + \Omega_Z\right)^2 + \left(u + \Omega_X\right)^2}} \\ \cos\alpha &= \frac{u + \Omega_X}{\sqrt{\left(w + \Omega_Z\right)^2 + \left(u + \Omega_X\right)^2}} \end{aligned}\right\} \tag{A30}$$

$$\left.\begin{aligned} \sin\beta &= \frac{v + \Omega_Y}{V_R} \\ \cos\beta &= \frac{\sqrt{\left(u + \Omega_X\right)^2 + \left(w + \Omega_Z\right)^2}}{V_R} \end{aligned}\right\} \tag{A31}$$

$$\left.\begin{aligned} \sin\gamma &= \frac{\dot{Z}_c}{\sqrt{\left(\dot{X}_c\right)^2 + \left(\dot{Y}_c\right)^2 + \left(\dot{Z}_c\right)^2}} \\ \cos\gamma &= \frac{\sqrt{\left(\dot{X}_c\right)^2 + \left(\dot{Y}_c\right)^2}}{\sqrt{\left(\dot{X}_c\right)^2 + \left(\dot{Y}_c\right)^2 + \left(\dot{Z}_c\right)^2}} \end{aligned}\right\} \tag{A32}$$

$$\left.\begin{aligned} h &= R - 20.9 \times 10^6 \text{ ft} \\ h &= R - 6.37 \times 10^6 \text{ m} \end{aligned}\right\} \tag{A33}$$

REFERENCES

1. Norman, Leland C.; McCullough, Jerry E.; and Coffey, Jerry C.: Gemini Land Landing System Development Program. Volume I – Full-Scale Investigations. NASA TN D-3869, 1967.
2. Layton, Garrison P., Jr.; and Thompson, Milton O.: Preliminary Flight Evaluation of Two Unpowered Manned Paragliders. NASA TN D-1826, 1963.
3. Libbey, Charles E.; Ware, George M.; and Naeseth, Rodger L.: Wind-Tunnel Investigation of the Static Aerodynamic Characteristics of an 18-Foot (5.49-Meter) All-Flexible Parawing. NASA TN D-3856, 1967.
4. Mechtly, E. A.: The International System of Units – Physical Constants and Conversion Factors. NASA SP-7012, 1964.
5. Kaestner, P. T.: An Articulated Optical Pickup for Scale Model Simulation. J. SMPTE, vol. 76, no. 10, Oct. 1967, pp. 988-991.
6. Johnson, Joseph L., Jr.: Low-Subsonic Flight Characteristics of a Model of a Supersonic-Airplane Configuration With a Parawing as a Landing Aid. NASA TN D-2031, 1963.
7. Chambers, Joseph R.; and Boisseau, Peter C.: A Theoretical Analysis of the Dynamic Lateral Stability and Control of a Parawing Vehicle. NASA TN D-3461, 1966.

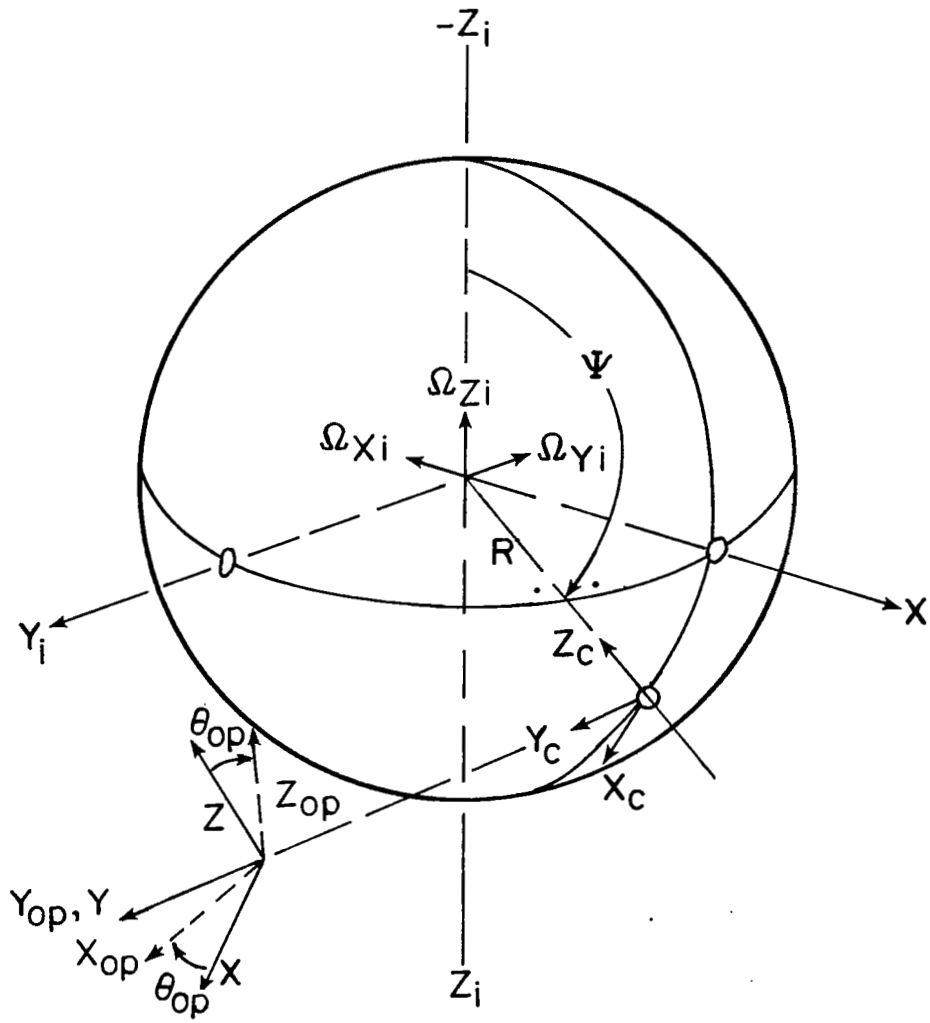

Figure 1.- Assumed axis systems and wind components.

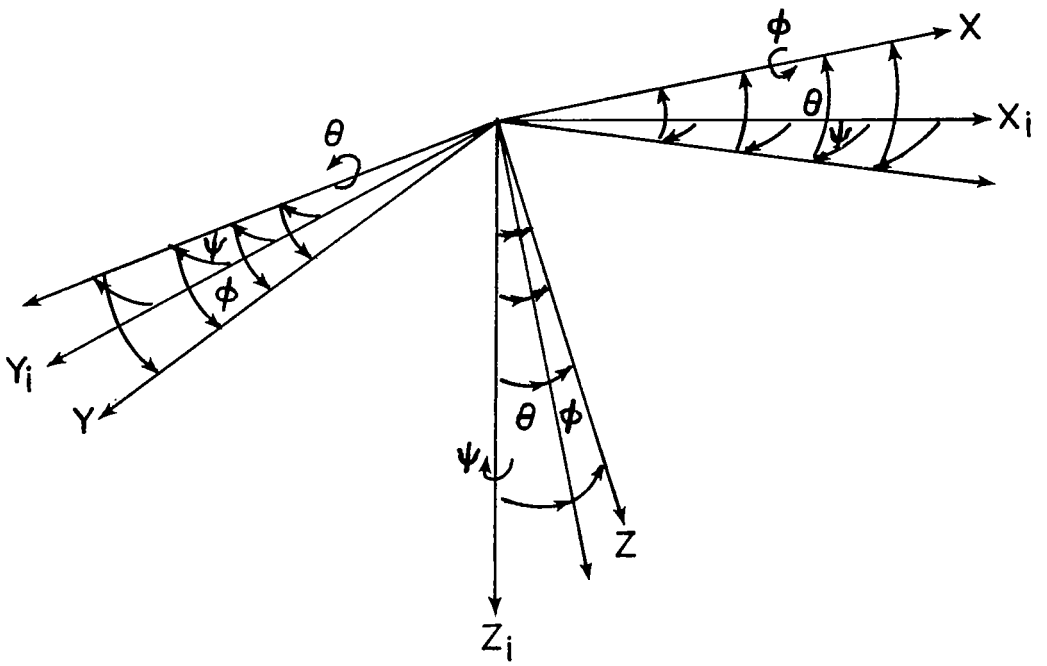

Figure 2.- Relation between body and inertial axes.

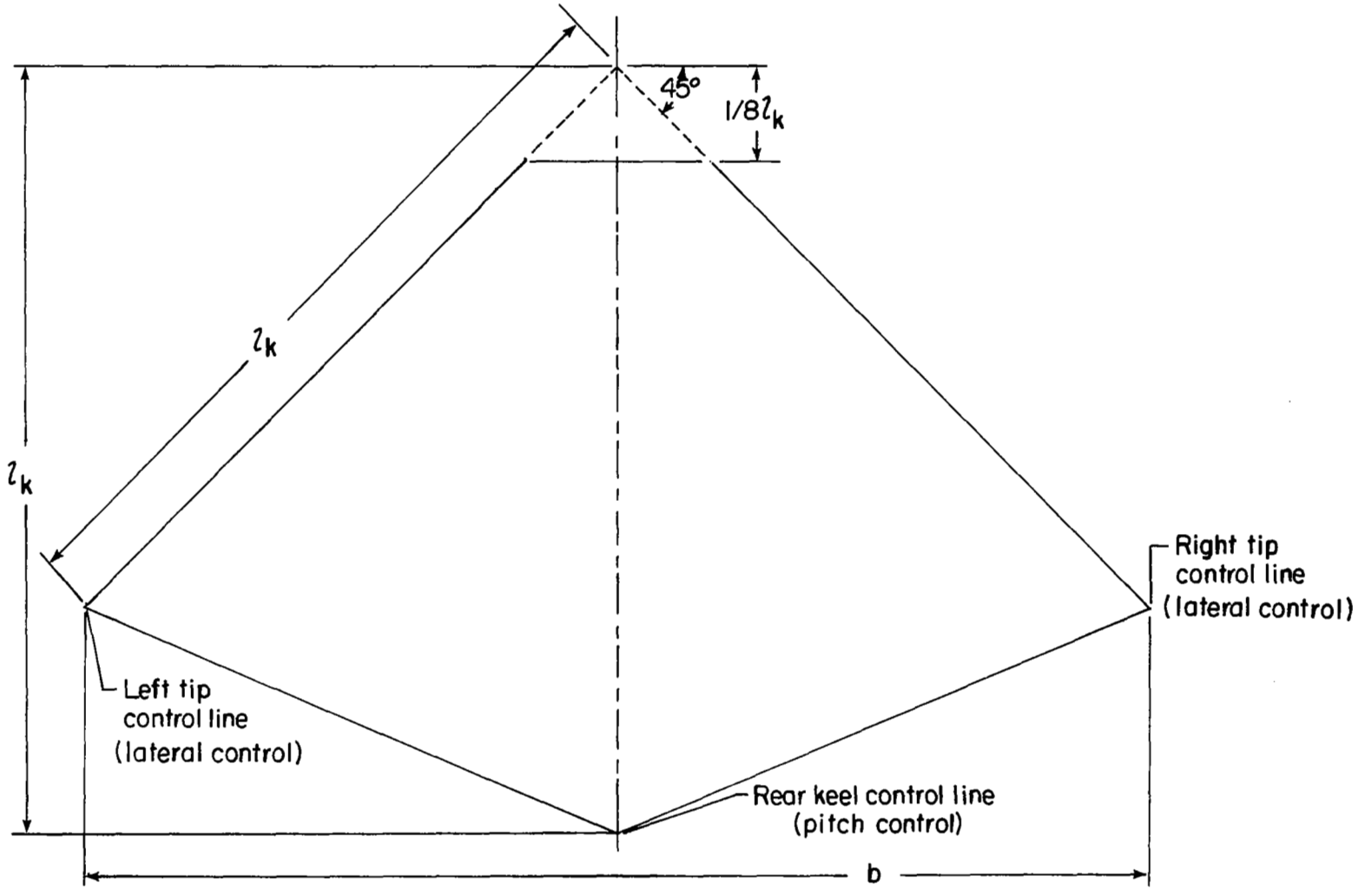

Figure 3.- Flat plan geometry of all-flexible parawing.

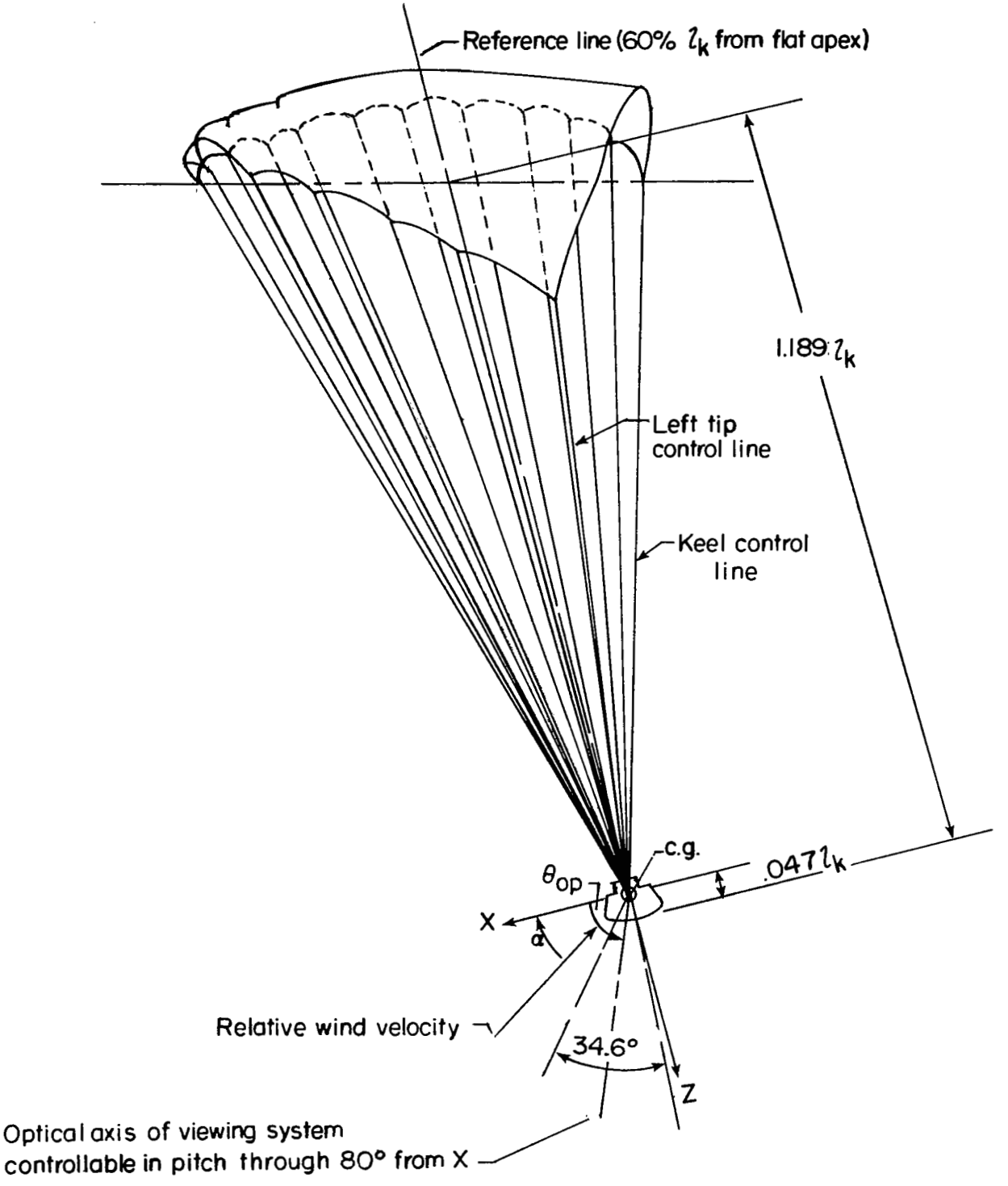

Figure 4.- Vehicle configuration.

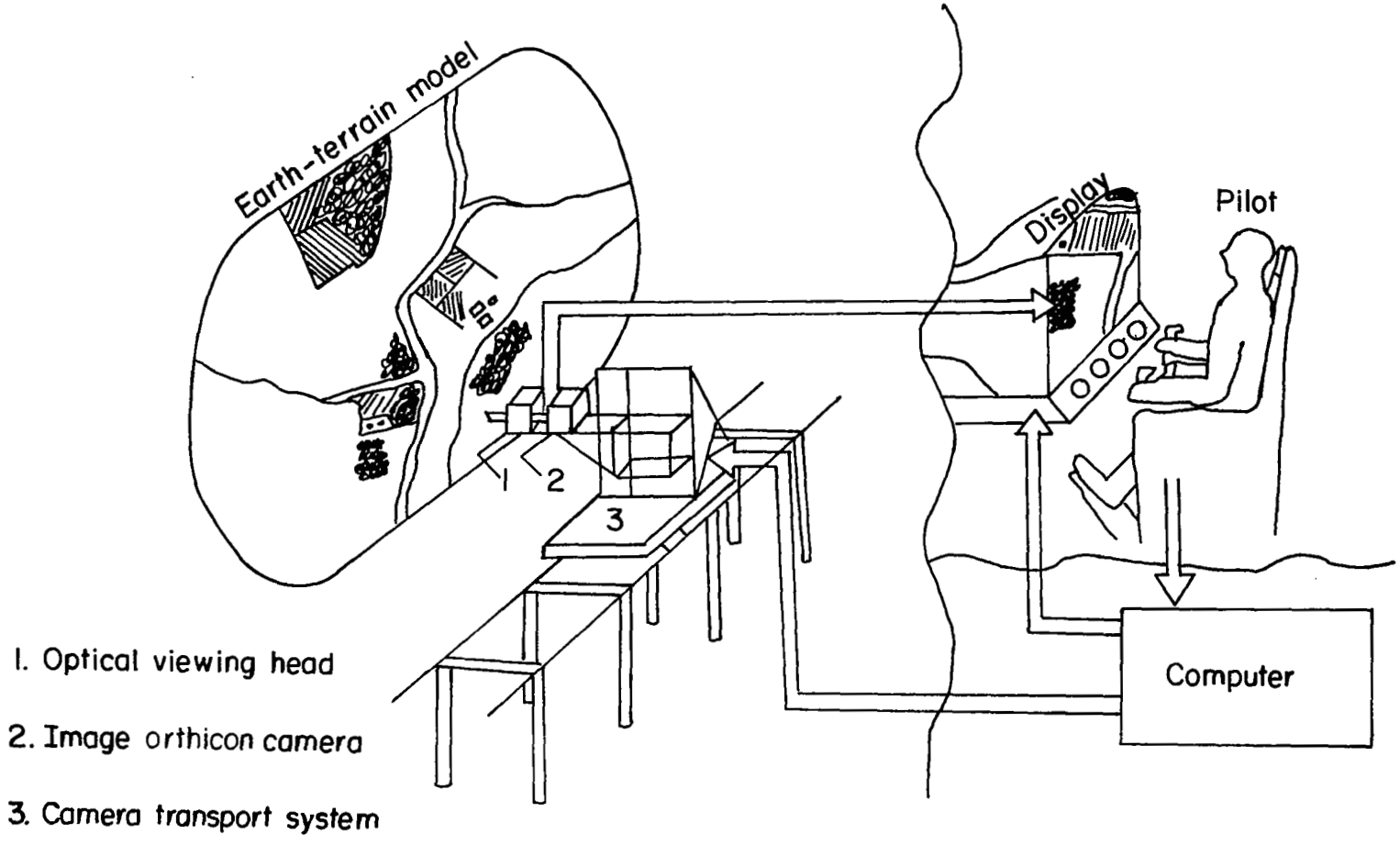

Figure 5.- Simulation equipment.

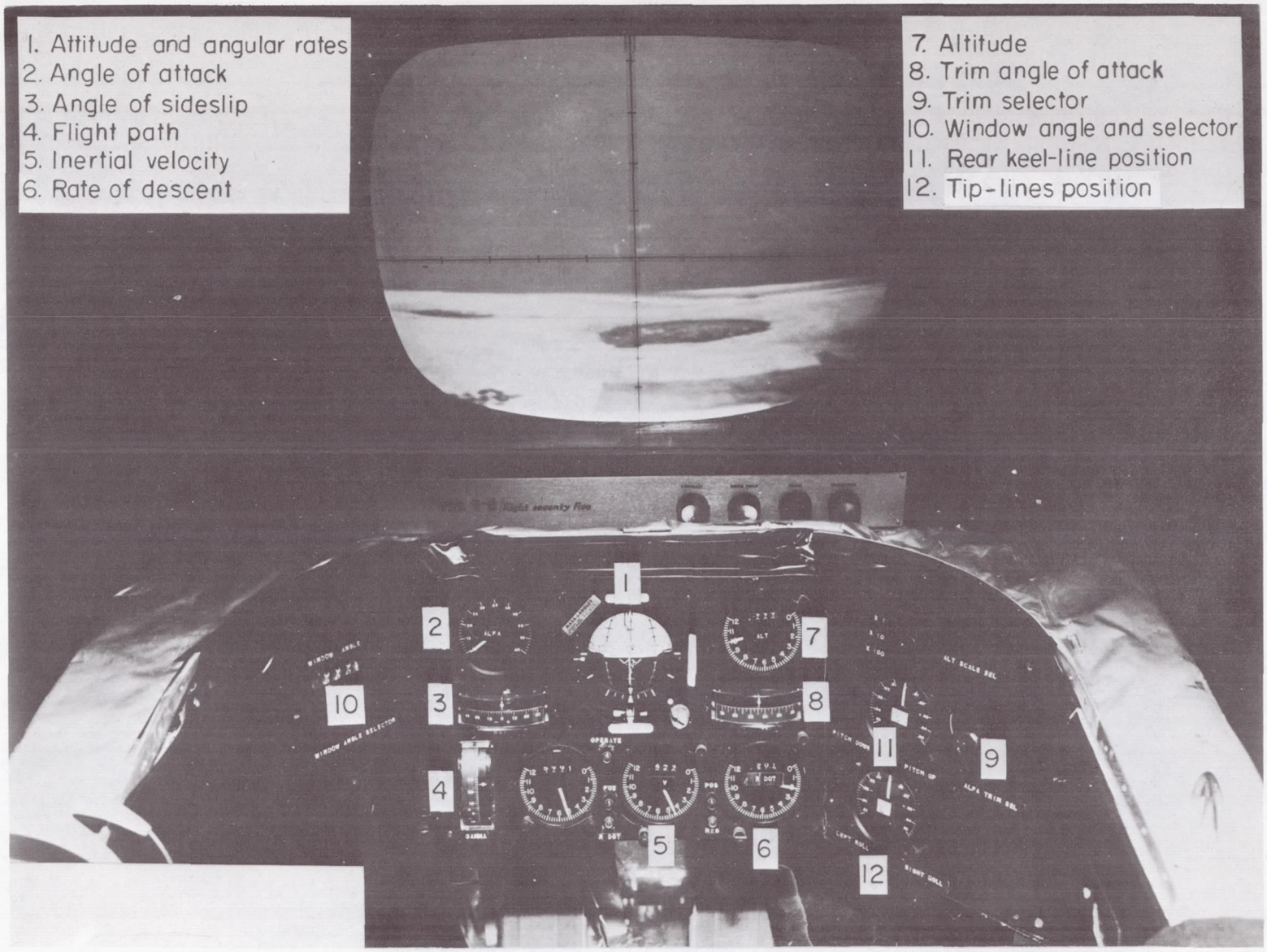

Figure 6.- Cockpit and instrumentation.

L-67-4666

1. Optical viewing head
2. Image orthicon camera
3. Camera transport system

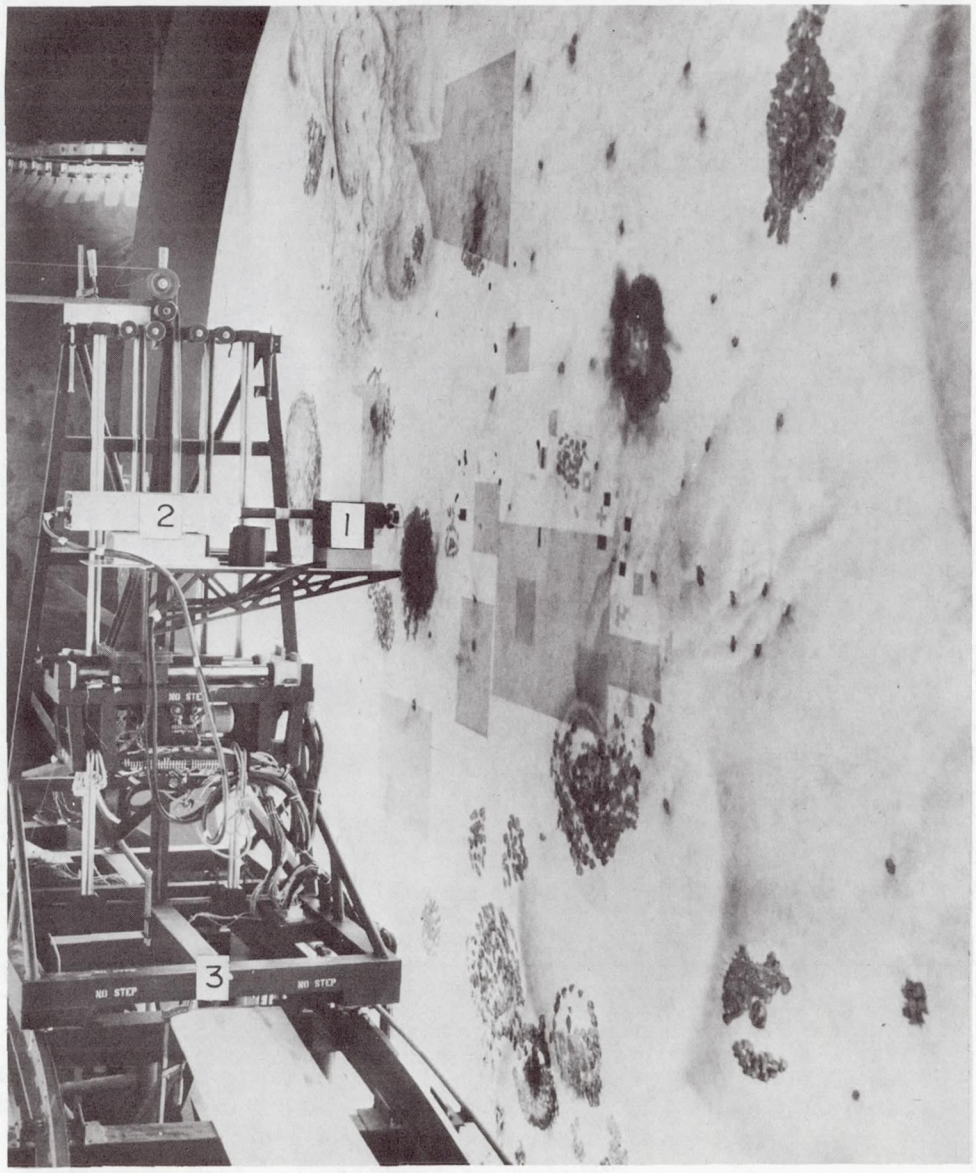

Figure 7.- Earth-terrain model and transport system. L-67-4664.1

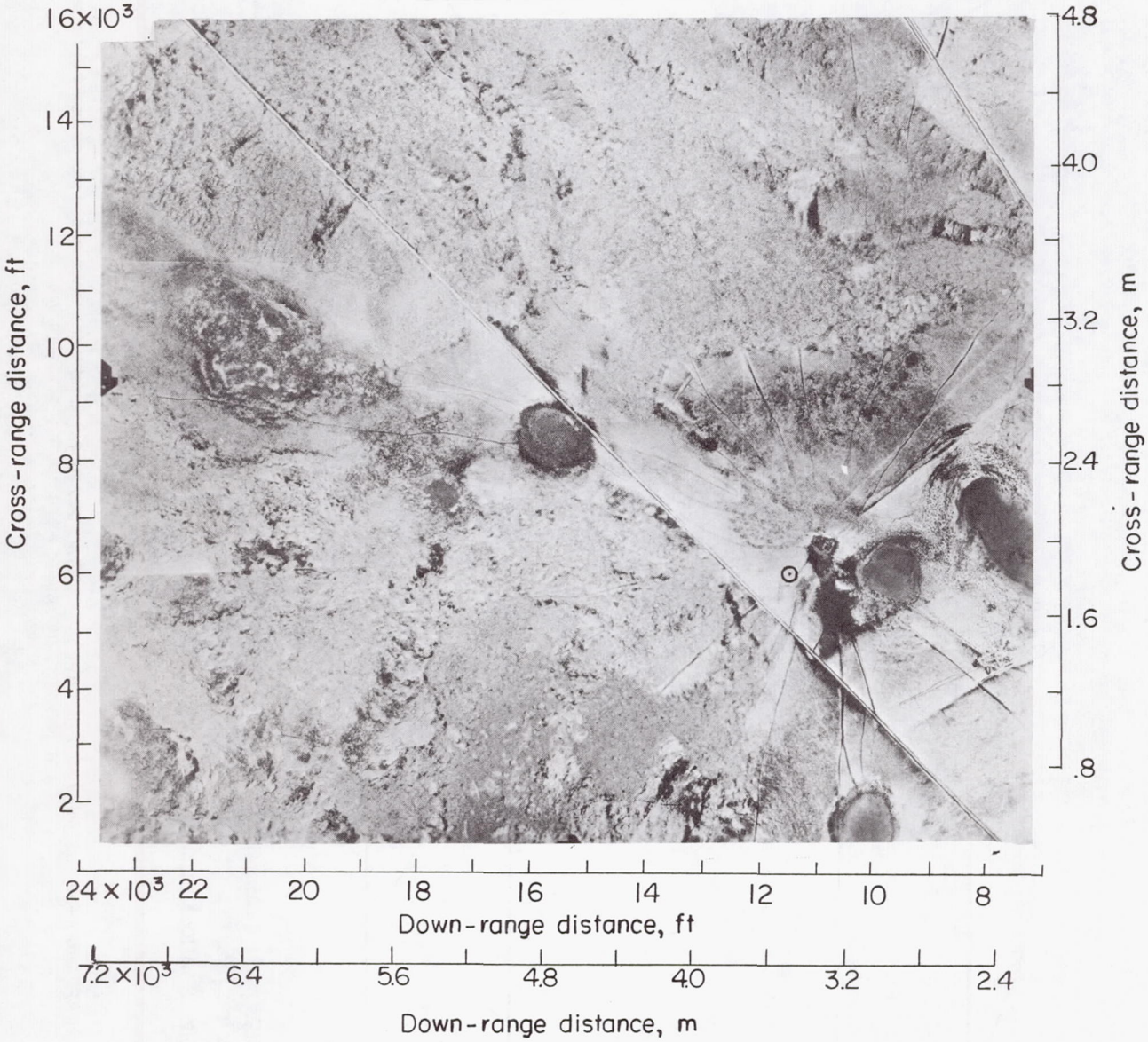

Figure 8.- Aerial photograph of landing site. (⊙ represents 300-foot-diameter (91.4-meter) landing site.) L-68-10,093

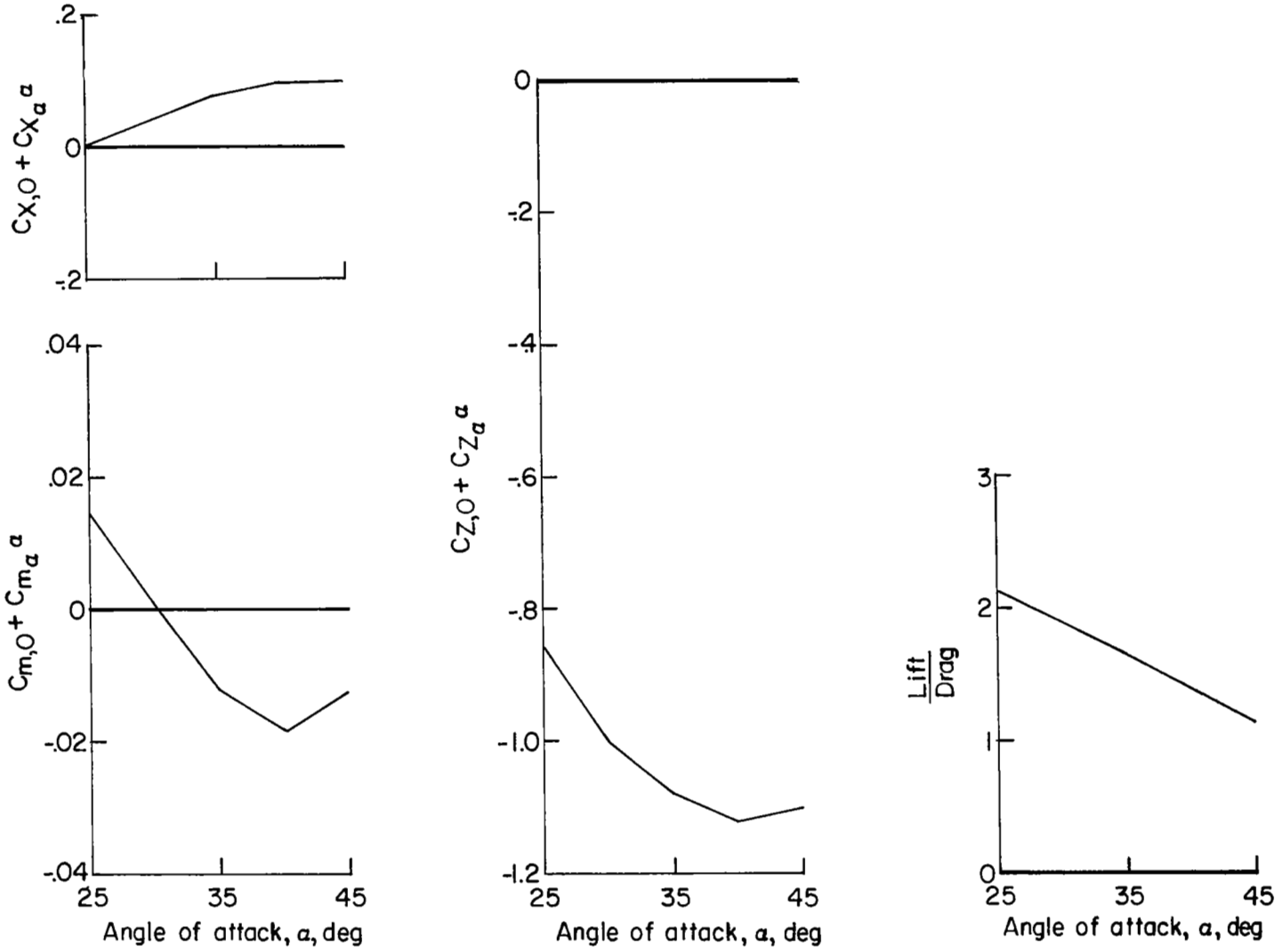

(a) Variation of $C_{X,0} + C_{X_\alpha}\alpha$, $C_{m,0} + C_{m_\alpha}\alpha$, $C_{Z,0} + C_{Z_\alpha}\alpha$, and Lift/Drag with α.

Figure 9.- Aerodynamic and control parameters used in simulation. Data are referenced to the body system of axes as located in figure 4. All parameters are based on area and span of wing when flat.

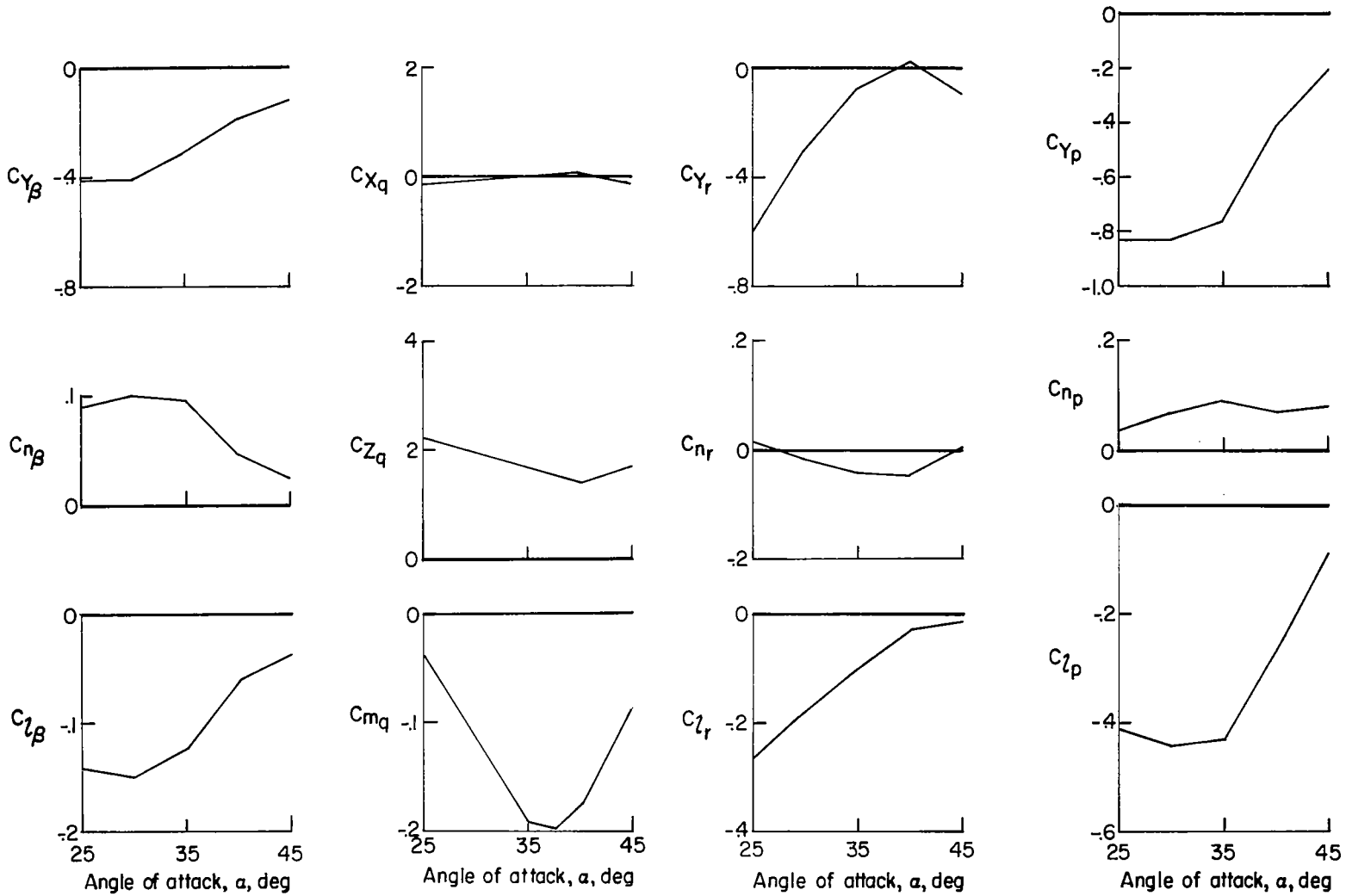

(b) Variation of the β, q, r, and p derivatives with α for undeflected controls. (These parameters are combination derivatives obtained from measurements made during forced oscillation tests of a 5-foot (1.52-meter) keel-length model described in the text.)

Figure 9.- Continued.

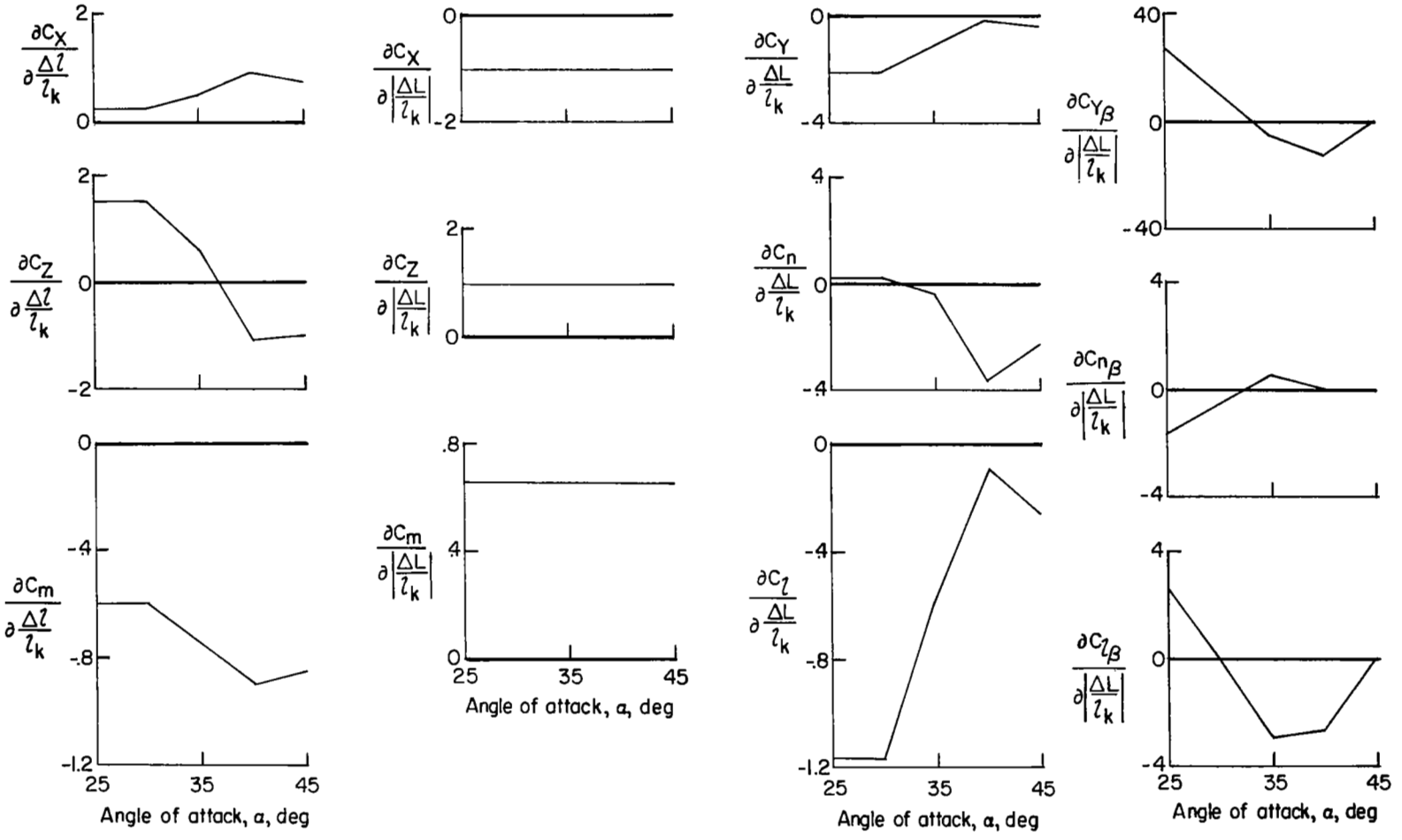

(c) Variation of control parameters with α.

Figure 9.- Concluded.

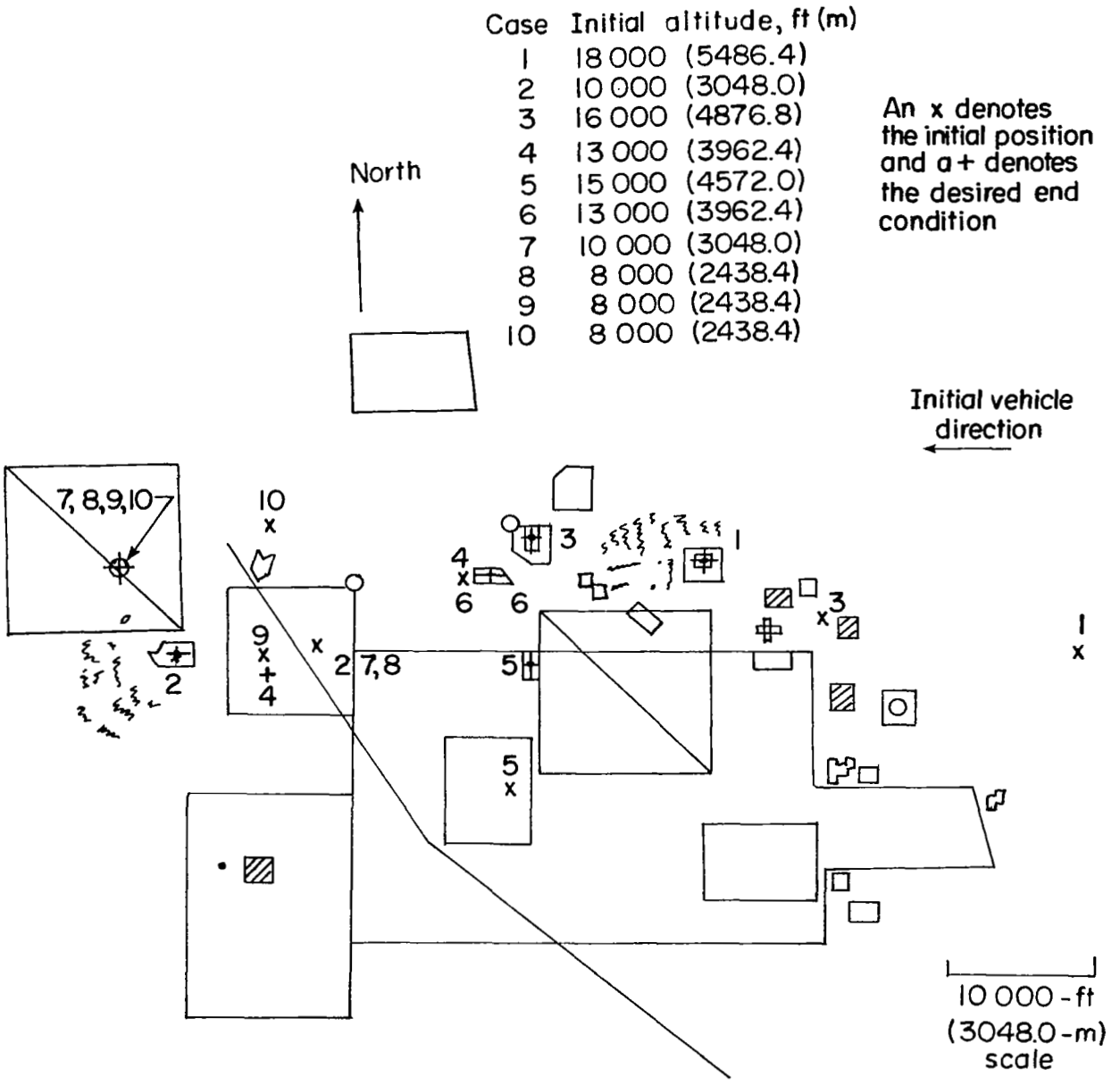

Figure 10.- Map of landing area.

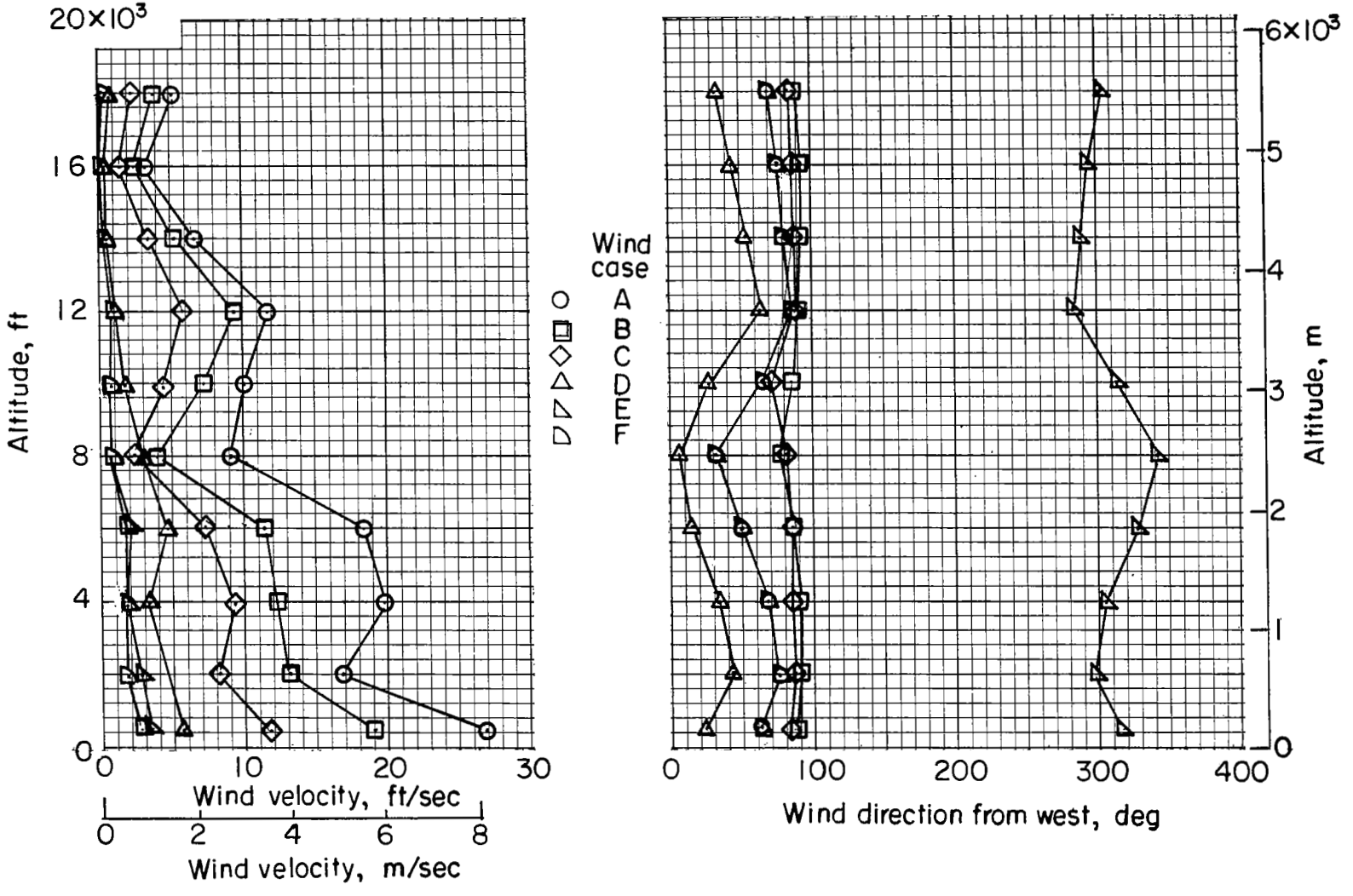

Figure 11.- Wind profiles.

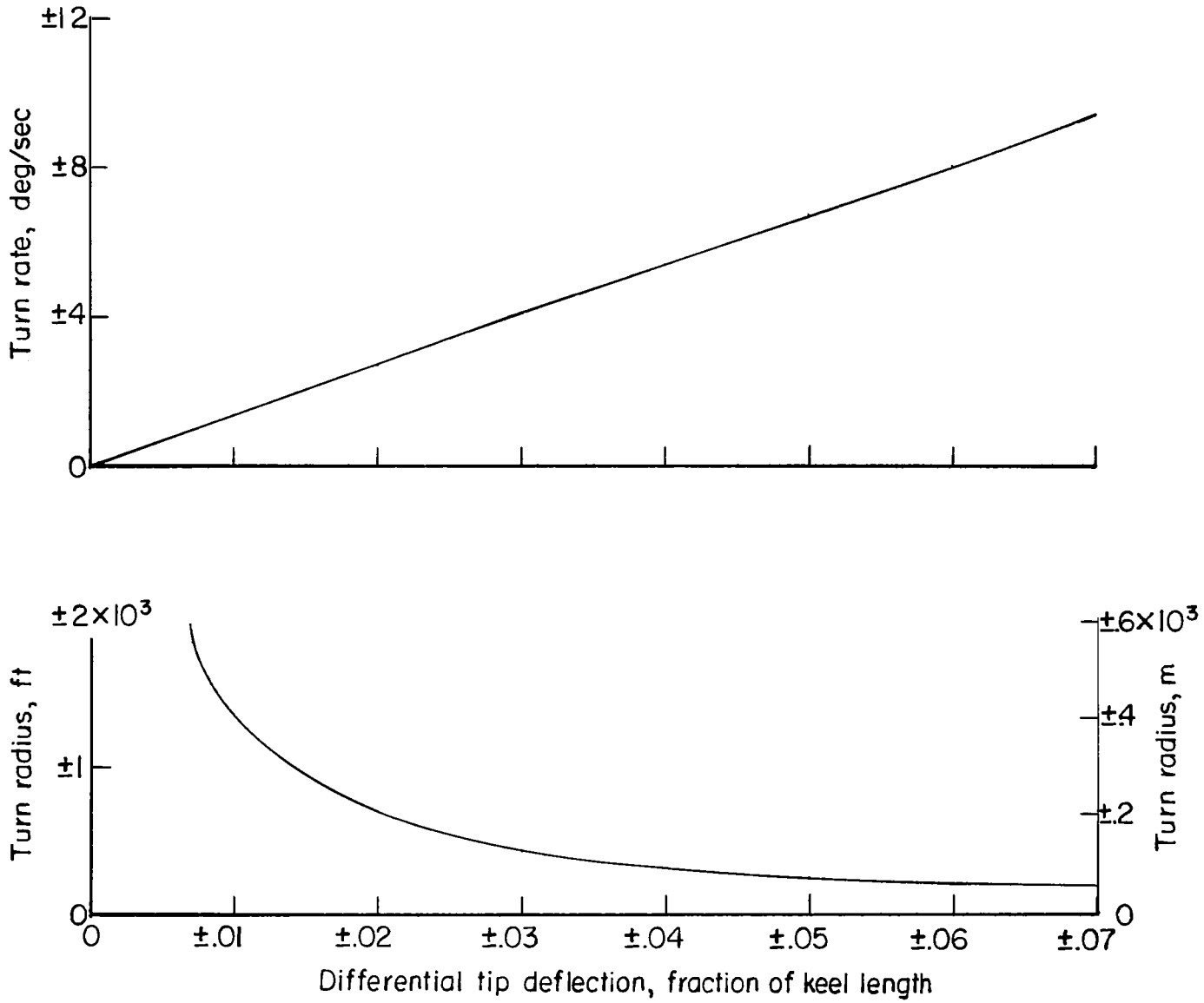

Figure 12.- Computed vehicle maneuvering capability in still air.

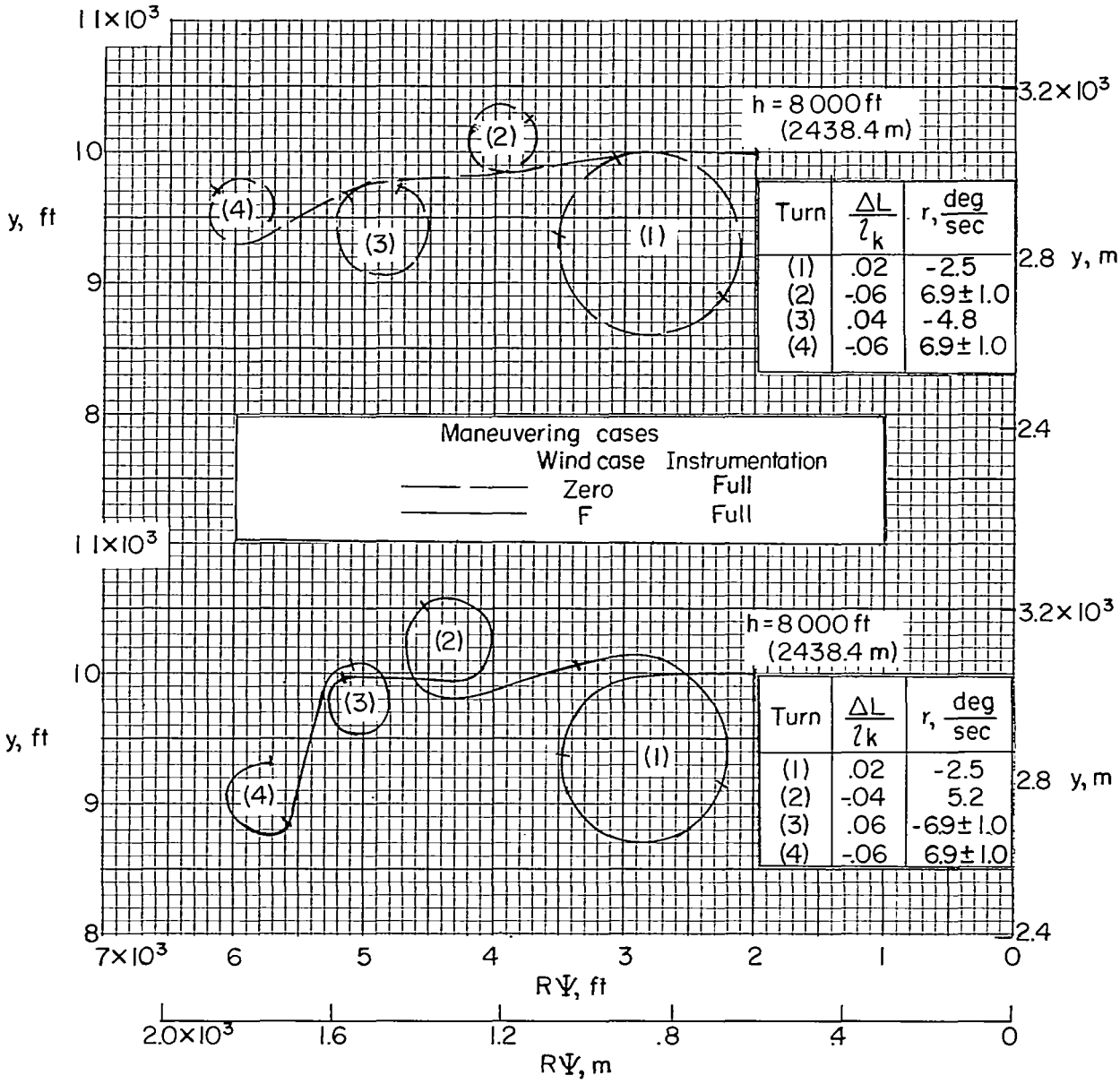

Figure 13.- Ground tracks showing vehicle maneuvering capability in still air and low winds. (Tick marks indicate 1000-foot (304.8-meter) increments in altitude decreasing from the indicated initial values.)

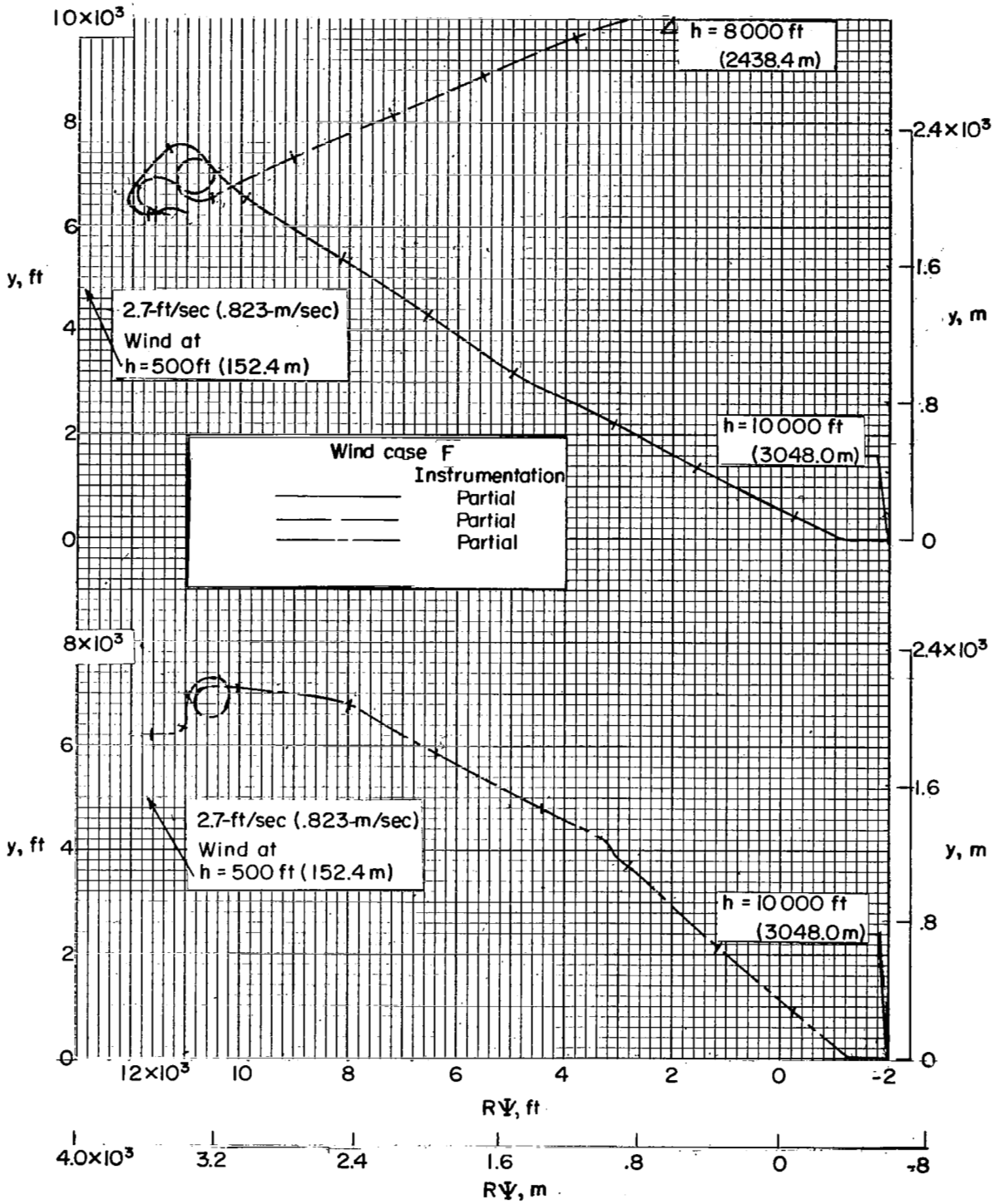

Figure 14.- Ground tracks of flights made under influence of low wind case F. (Tick marks indicate 1000-foot (304.8-meter) increments in altitude decreasing from the indicated initial values.)

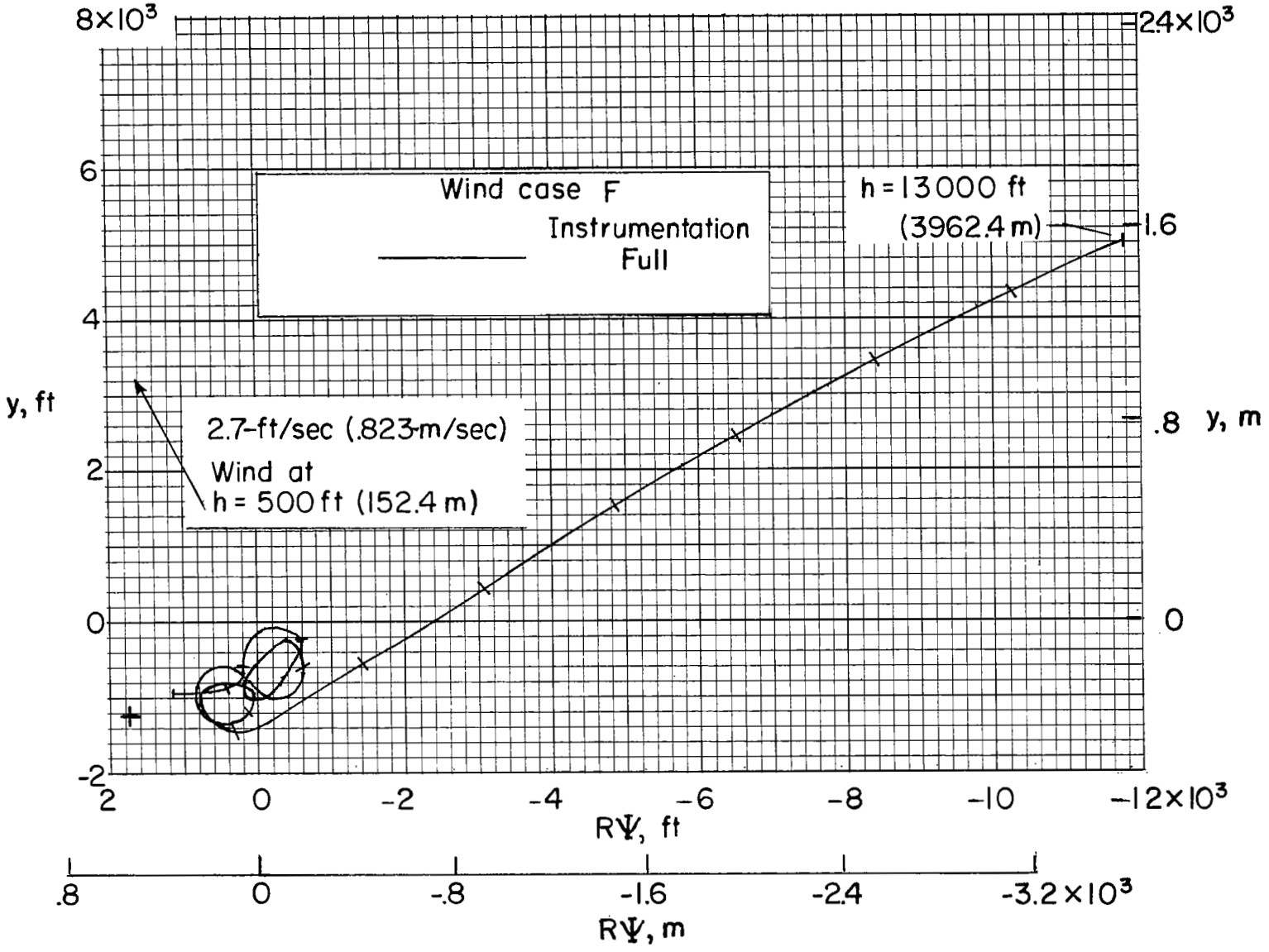

Figure 14.- Concluded.

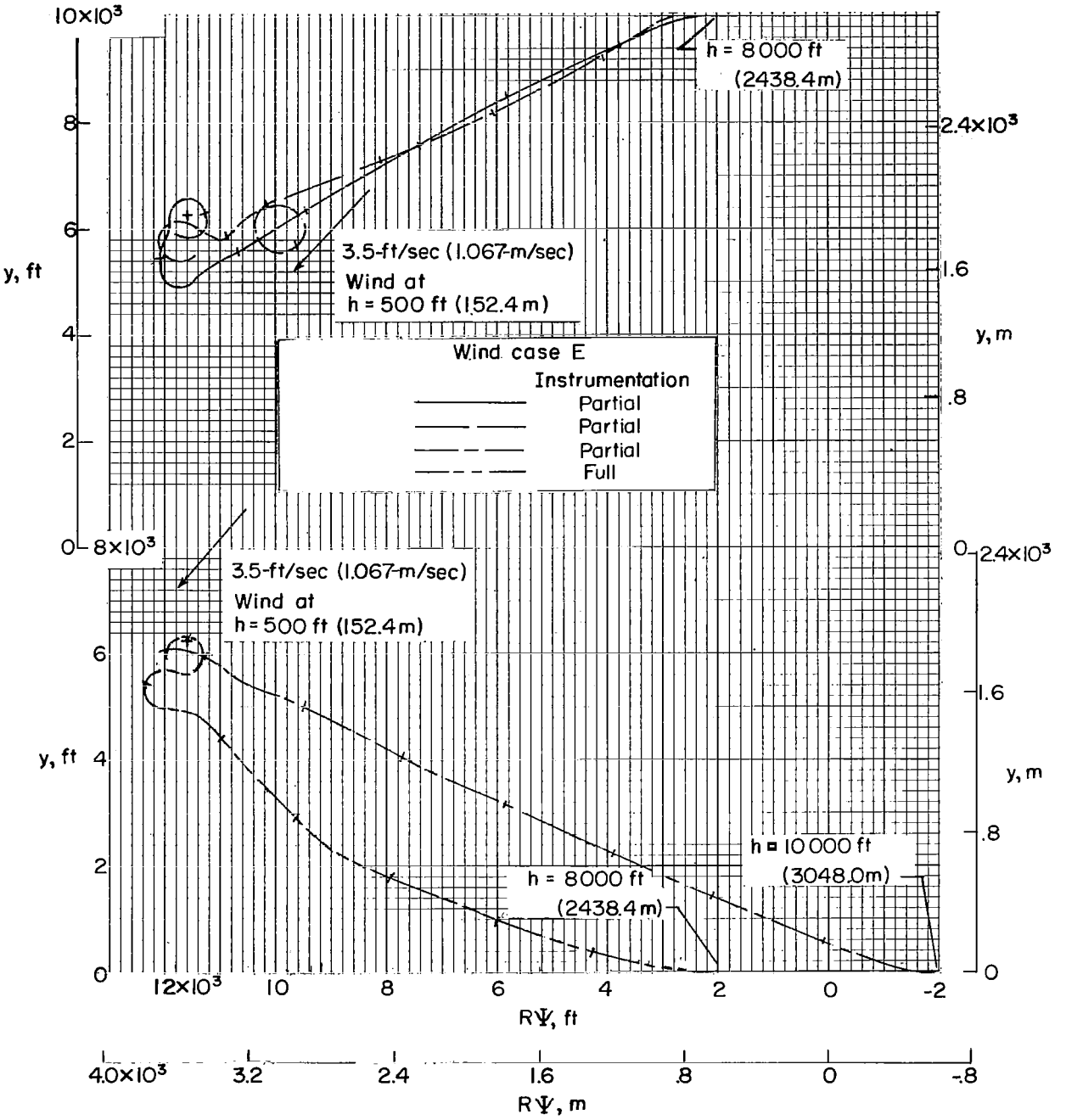

Figure 15.- Ground tracks of flights made under influence of low wind case E. (Tick marks indicate 1000-foot (304.8-meter) increments in altitude decreasing from the indicated initial values.)

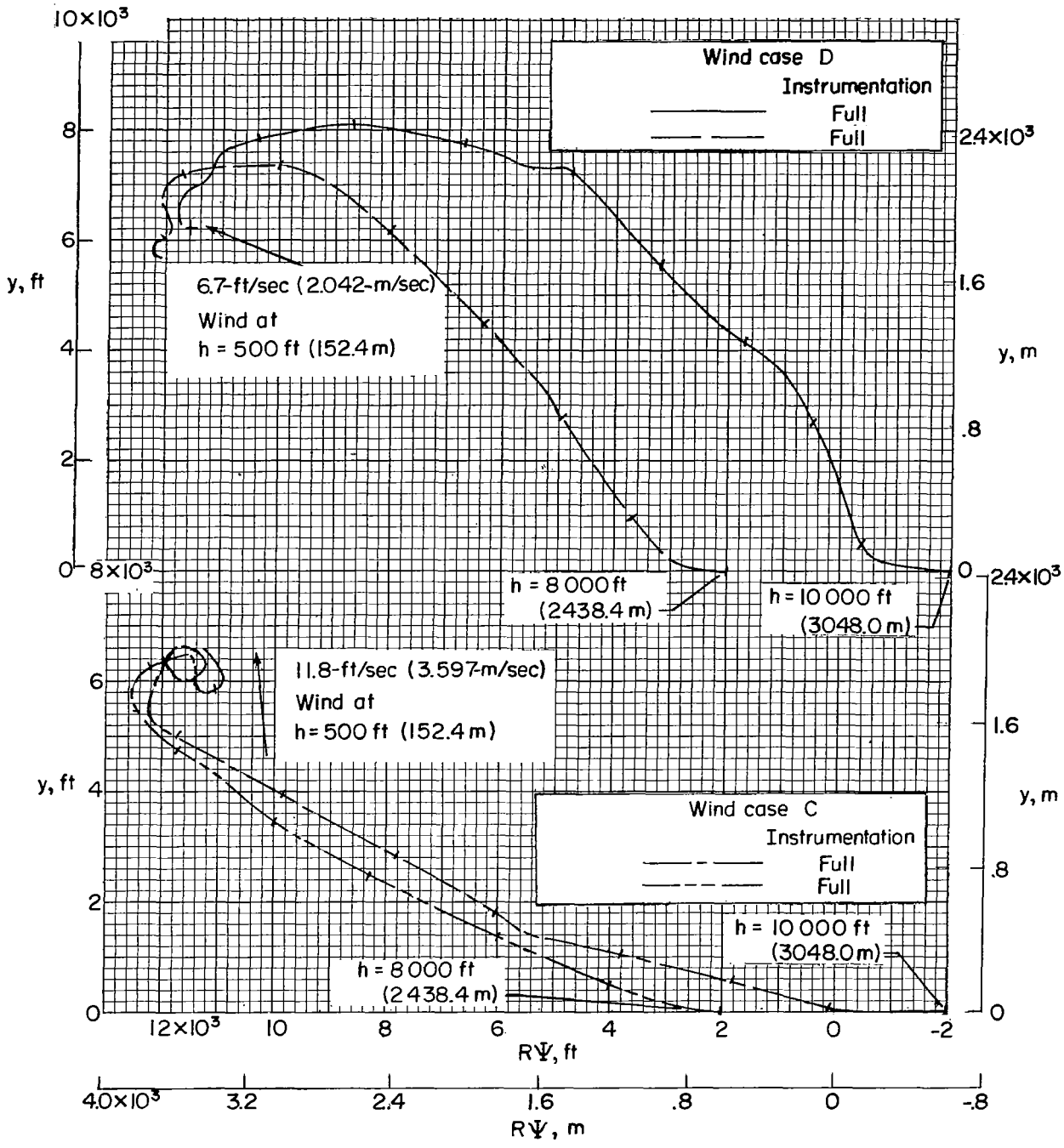

Figure 16.- Ground tracks of flights made under influence of low wind cases D and C. (Tick marks indicate 1000-foot (304.8-meter) increments in altitude decreasing from the indicated initial values.)

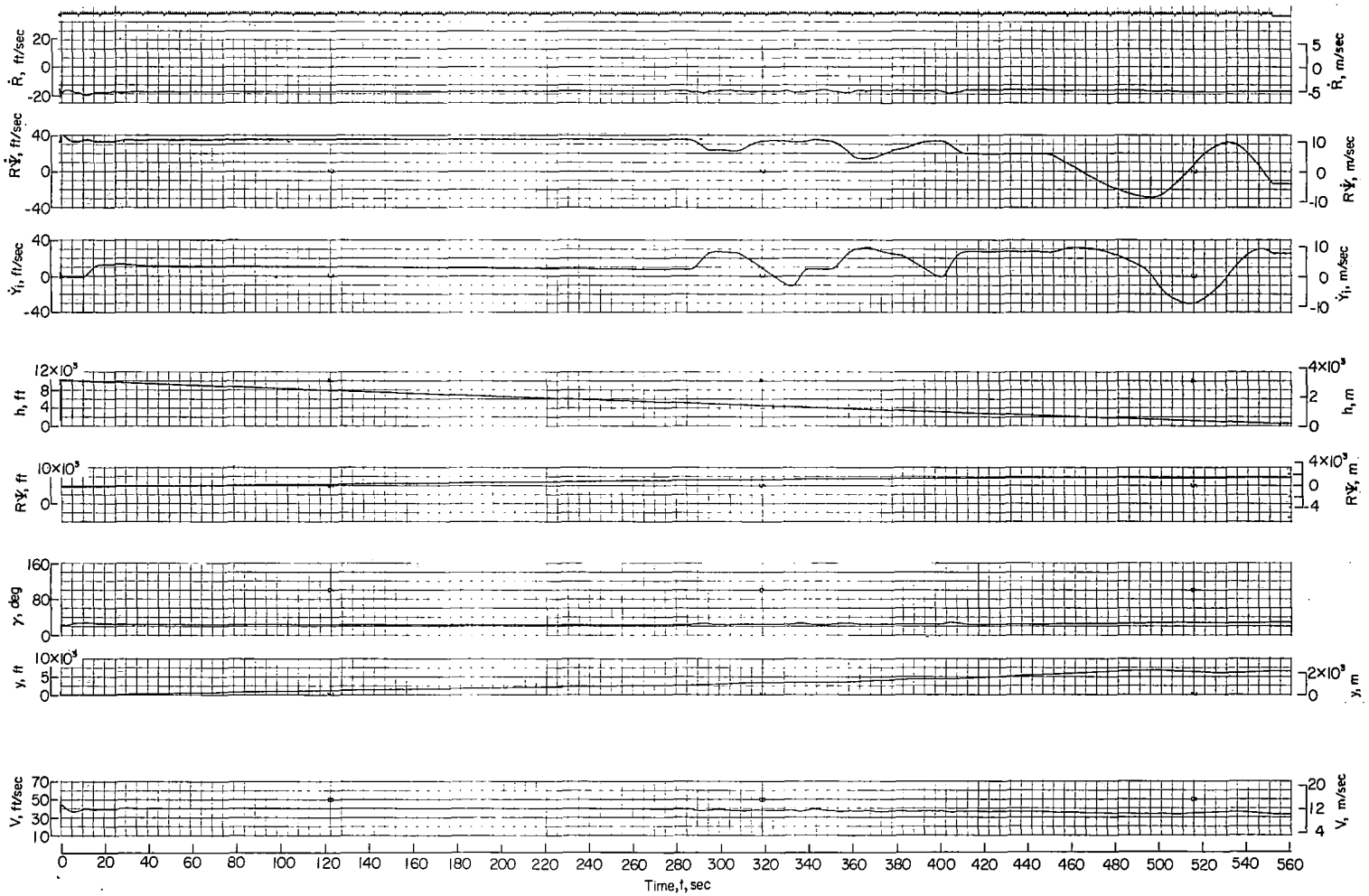

Figure 17.- Time history of typical flight under the influence of low wind case E.

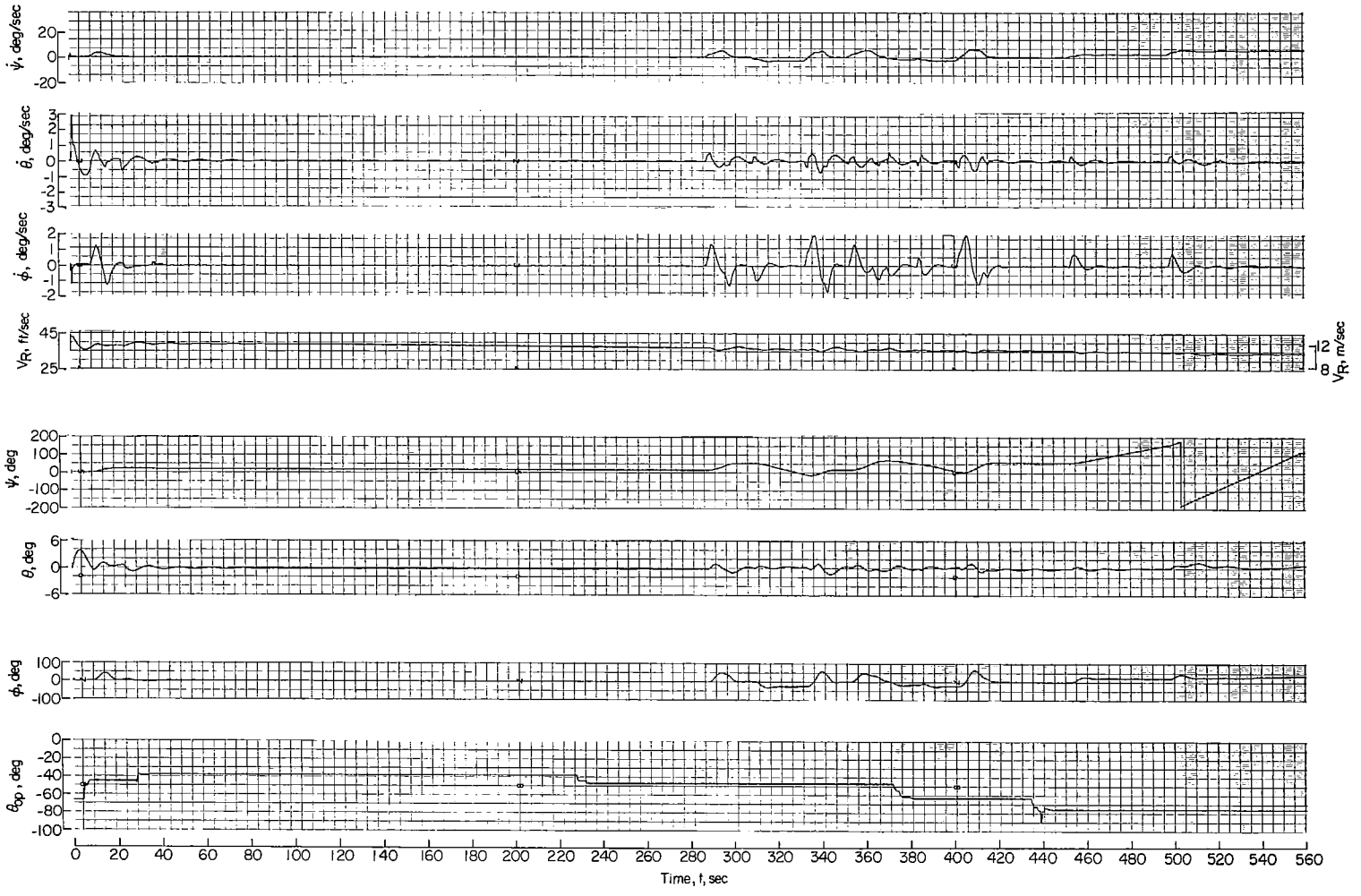

Figure 17.- Continued.

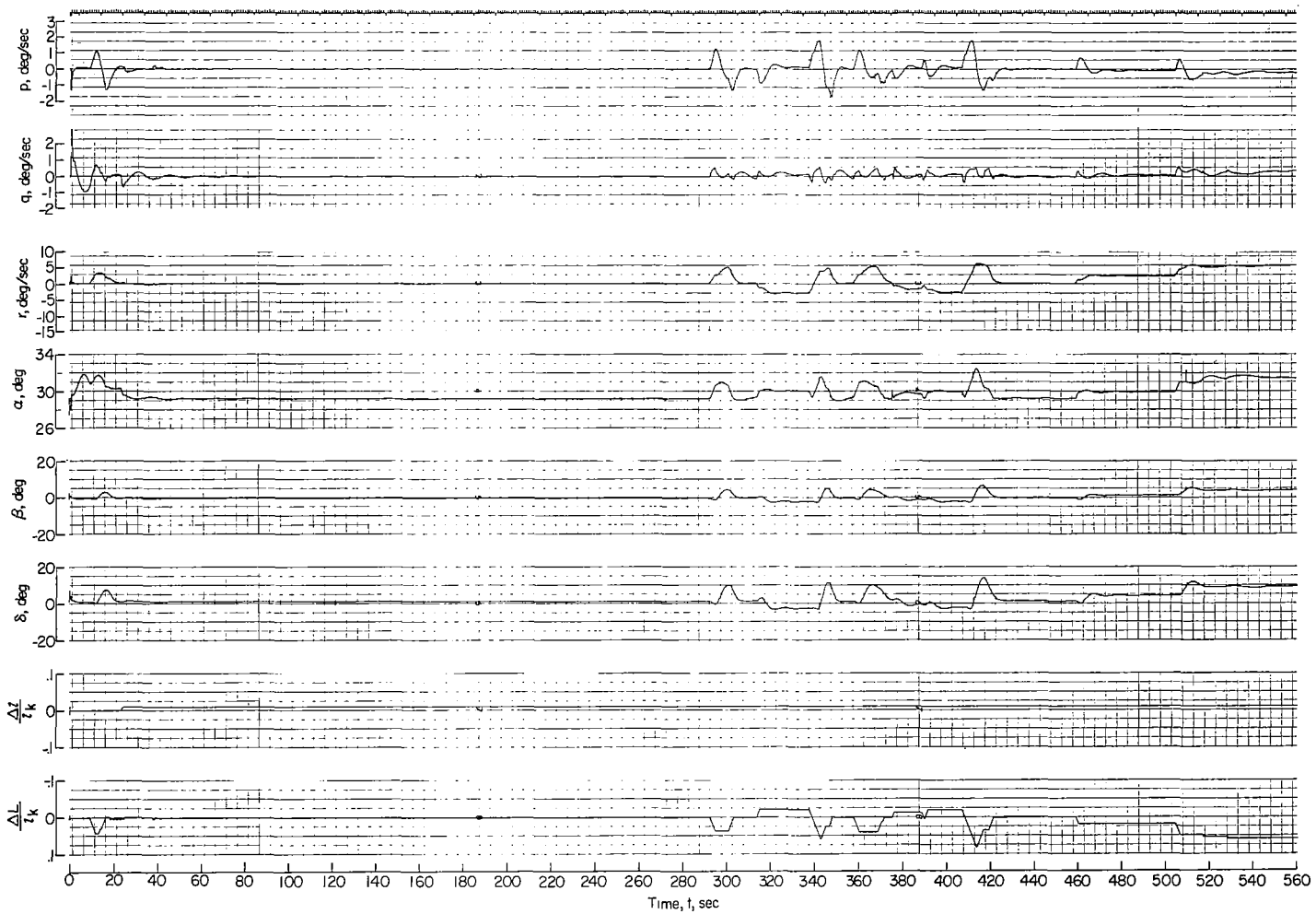

Figure 17.- Continued.

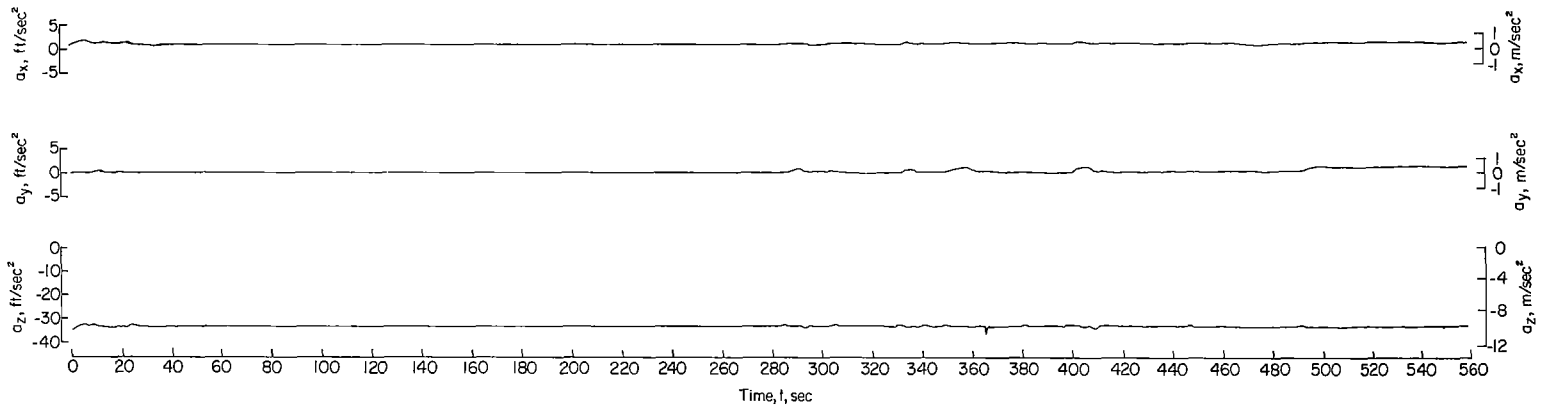

Figure 17.- Concluded.

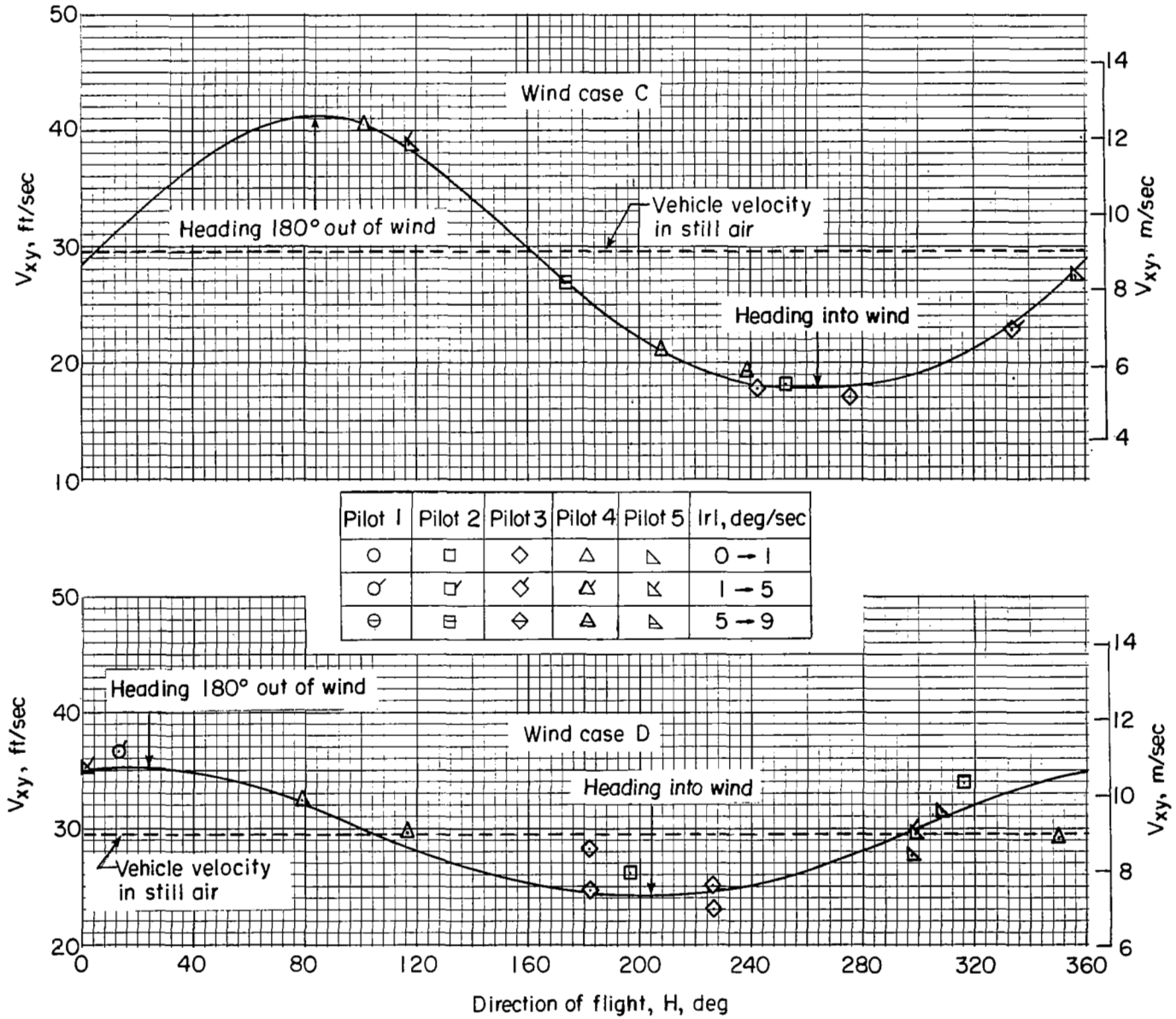

Figure 18.- Terminal ground speed, direction of flight, and turn rate for flights made in low winds.

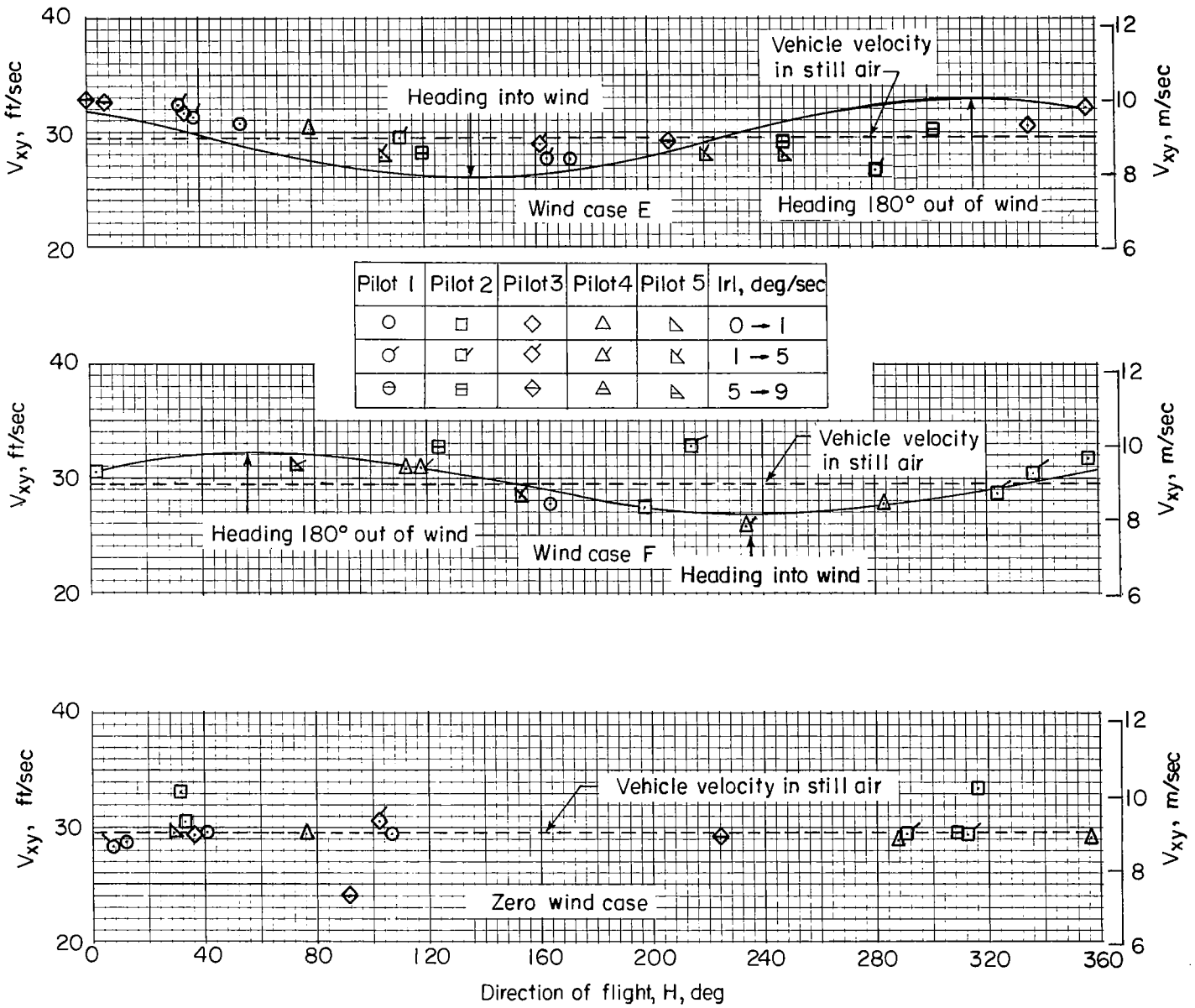

Figure 18.- Concluded.

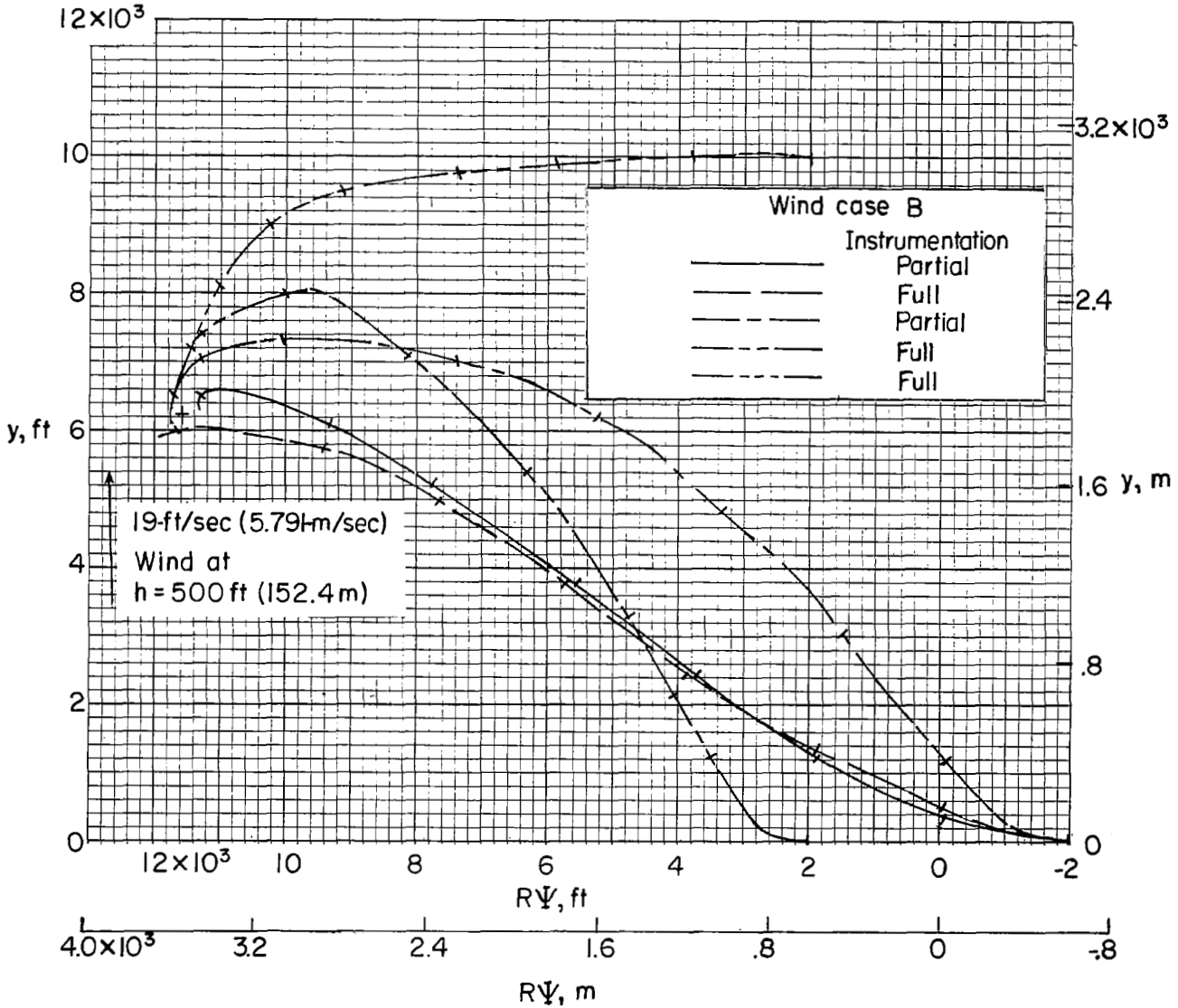

(a) Tick marks indicate 1000-foot (304.8-meter) increments in altitude decreasing from an initial altitude of 8000 feet (2438.4 meters).

Figure 19.- Ground tracks of flights made under influence of high wind case B.

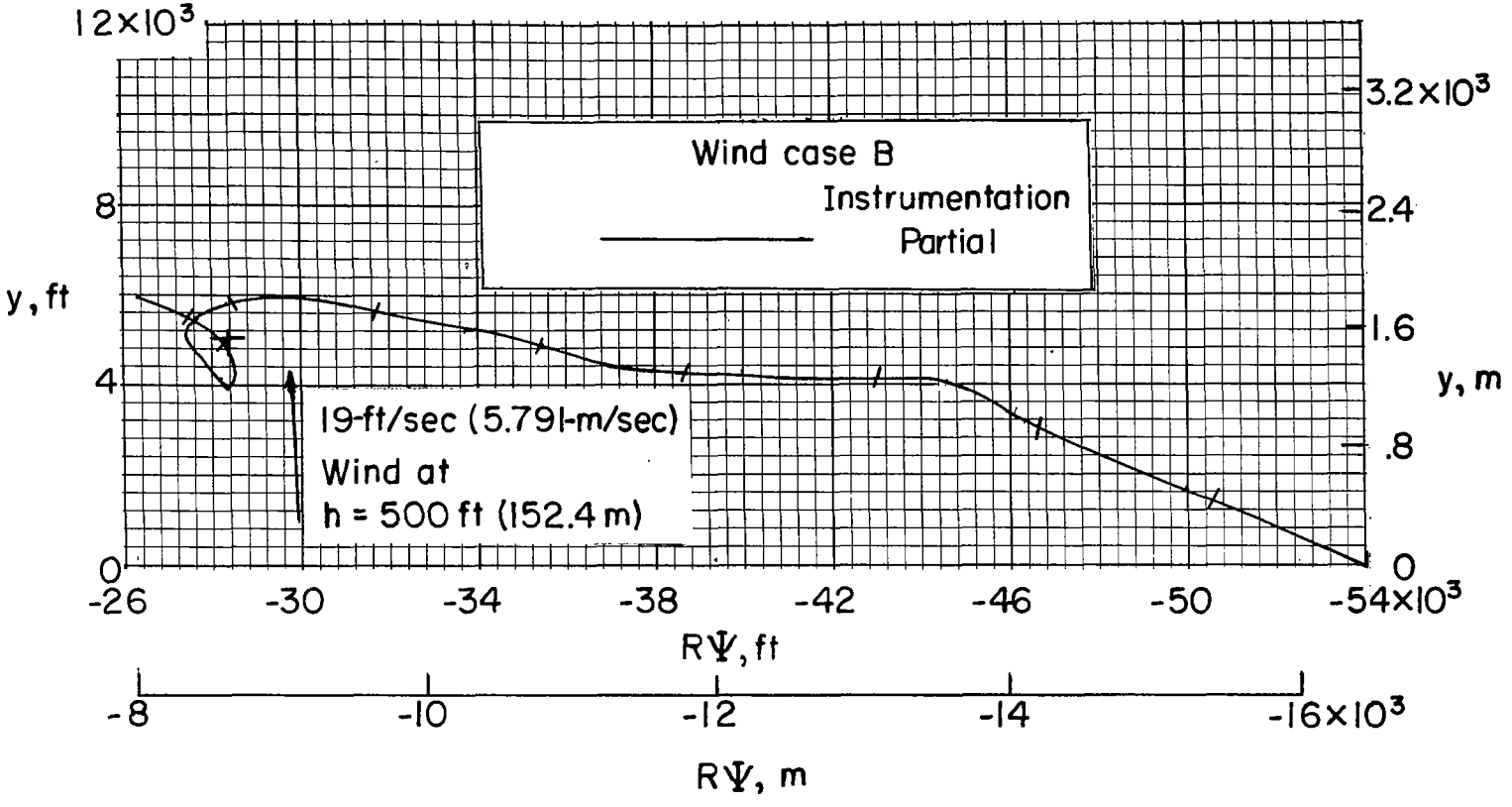

(b) Tick marks indicate 2000-foot (609.6-meter) increments in altitude decreasing from an initial altitude of 18 000 feet (5486.4 meters).

Figure 19.- Concluded.

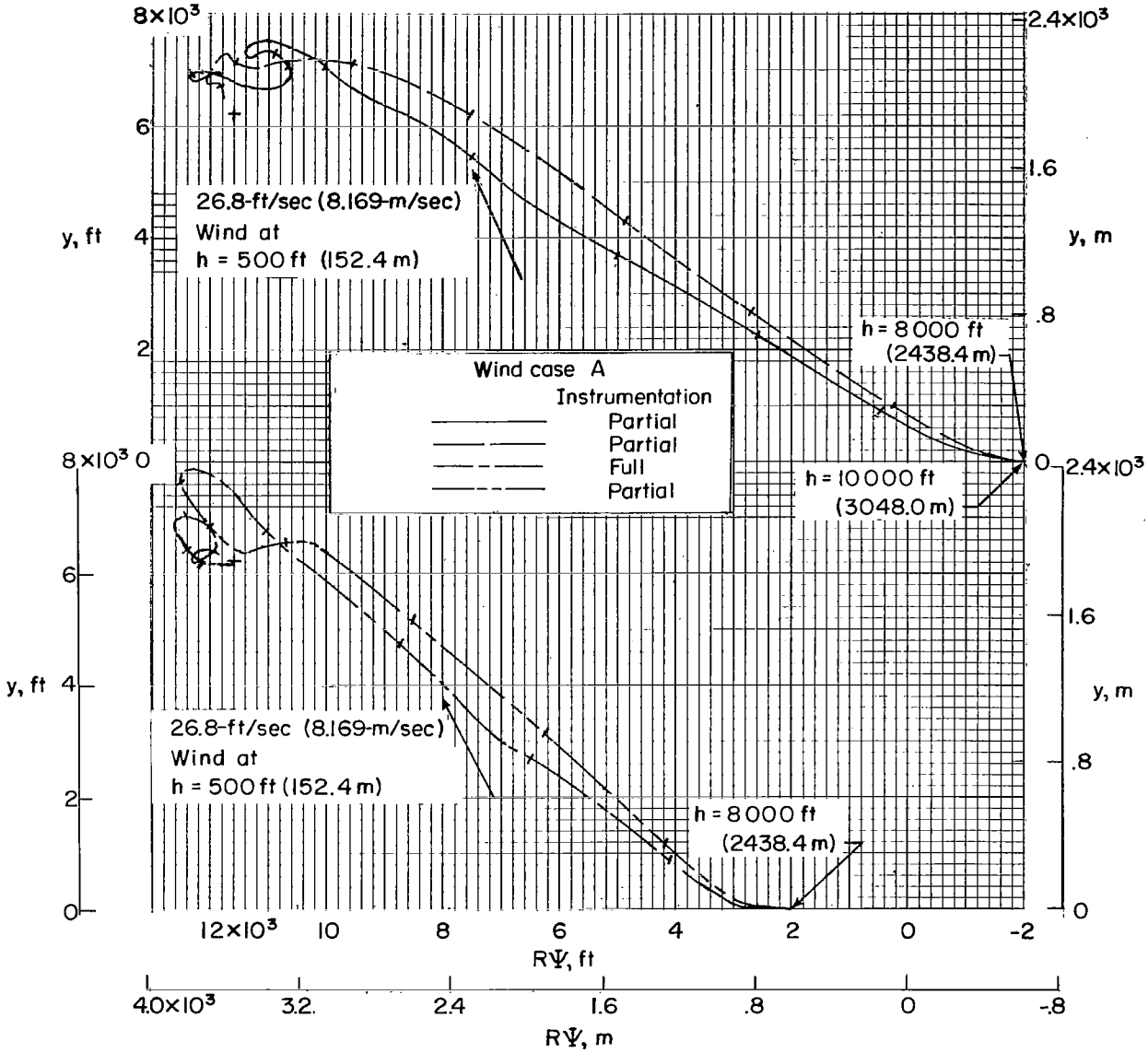

Figure 20.- Ground tracks of flights made under influence of high wind case A. (Tick marks indicate 1000-foot (304.8-meter) increments in altitude decreasing from the indicated initial values.)

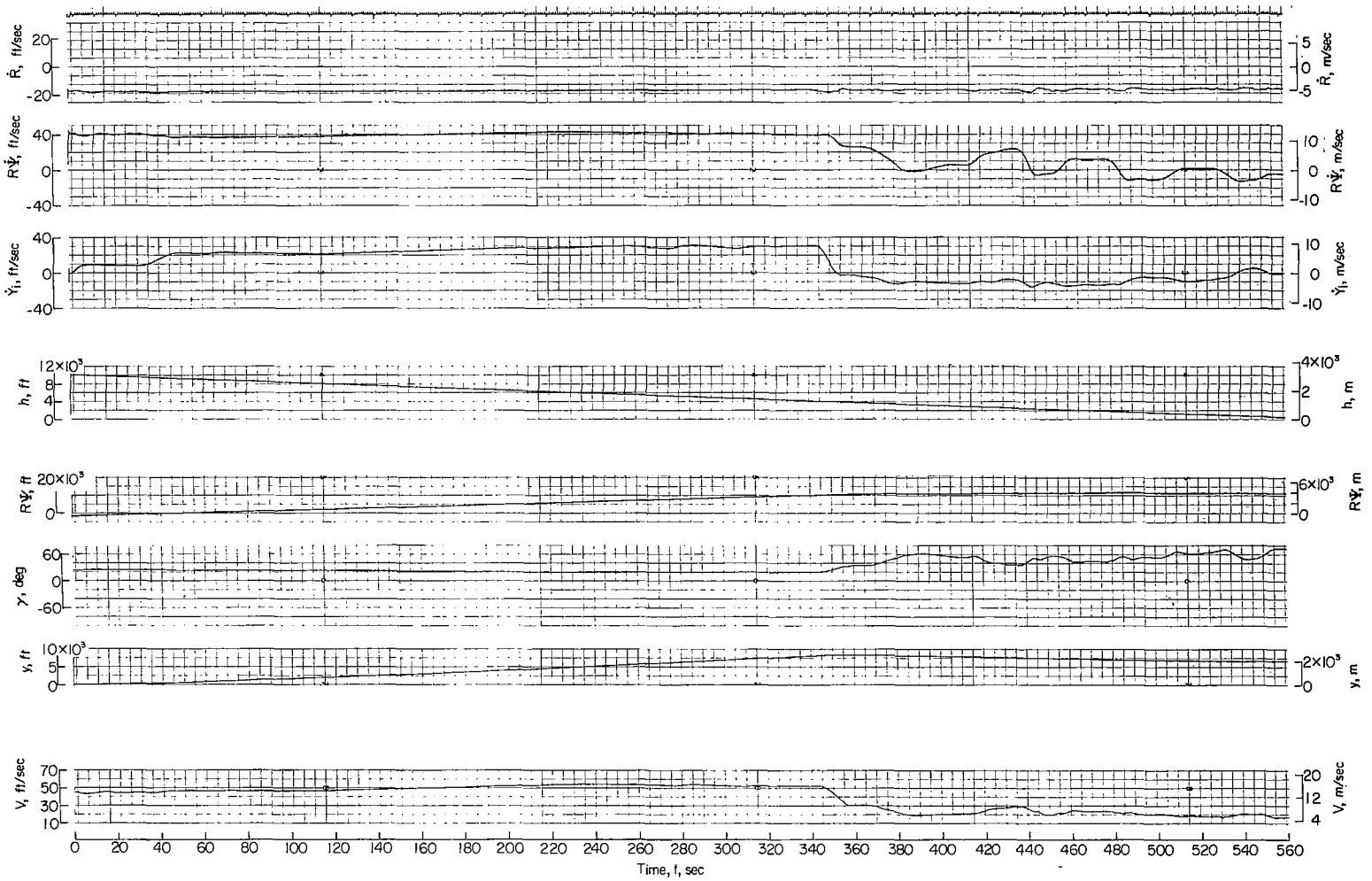

Figure 21.- Time history of typical flight under the influence of high wind case A.

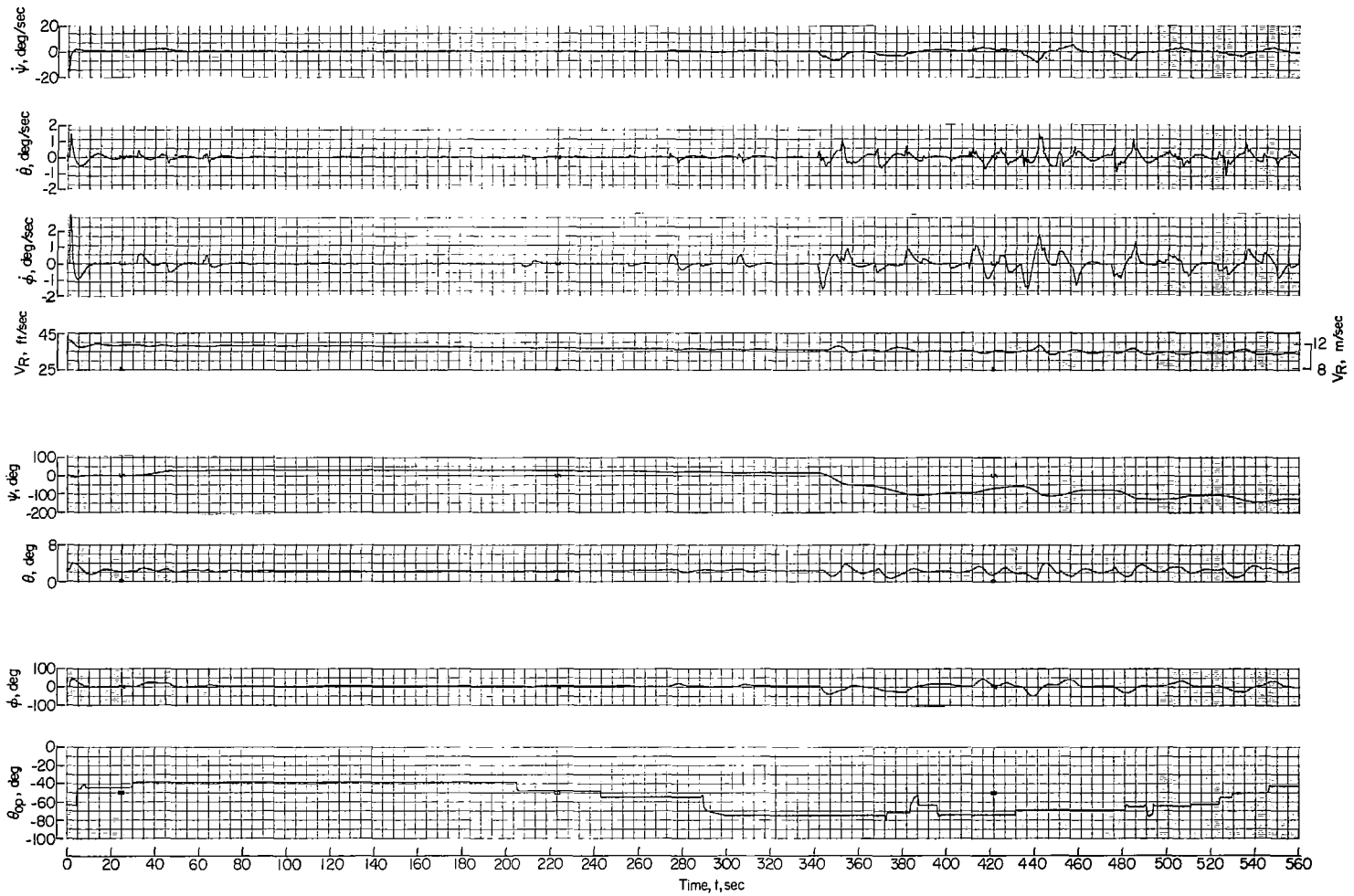

Figure 21.- Continued.

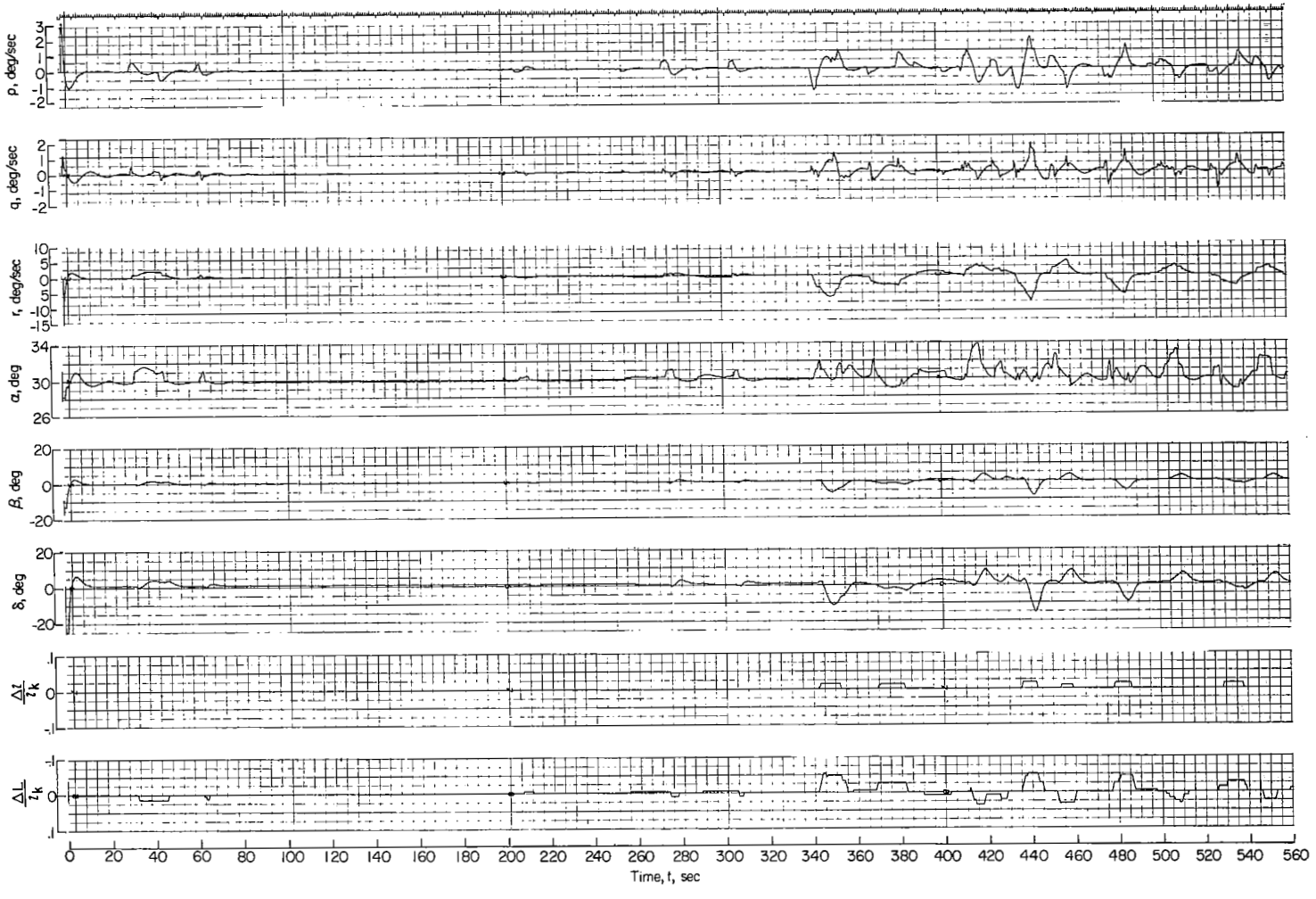

Figure 21.- Continued.

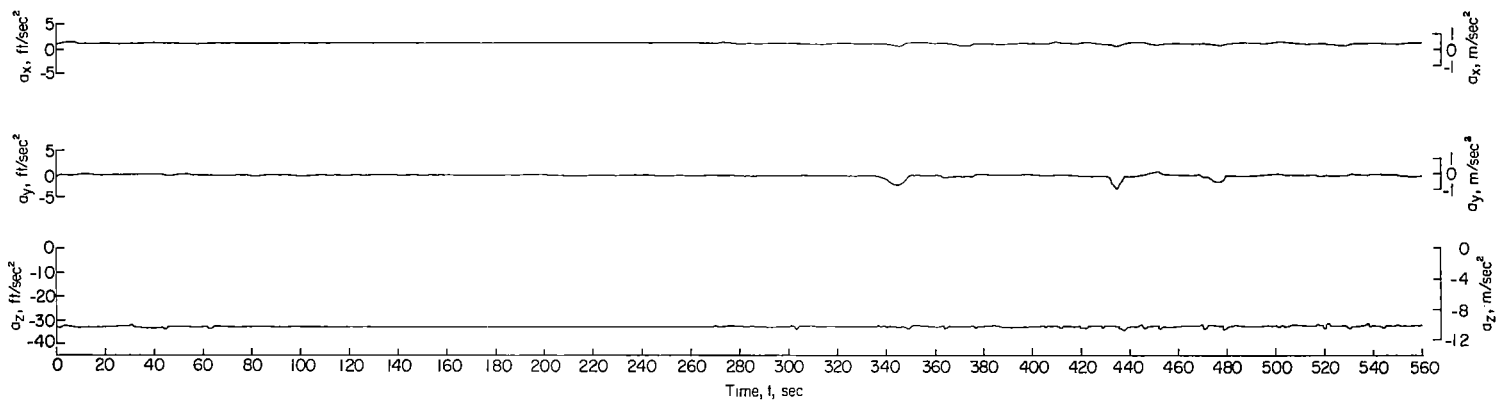

Figure 21.- Concluded.

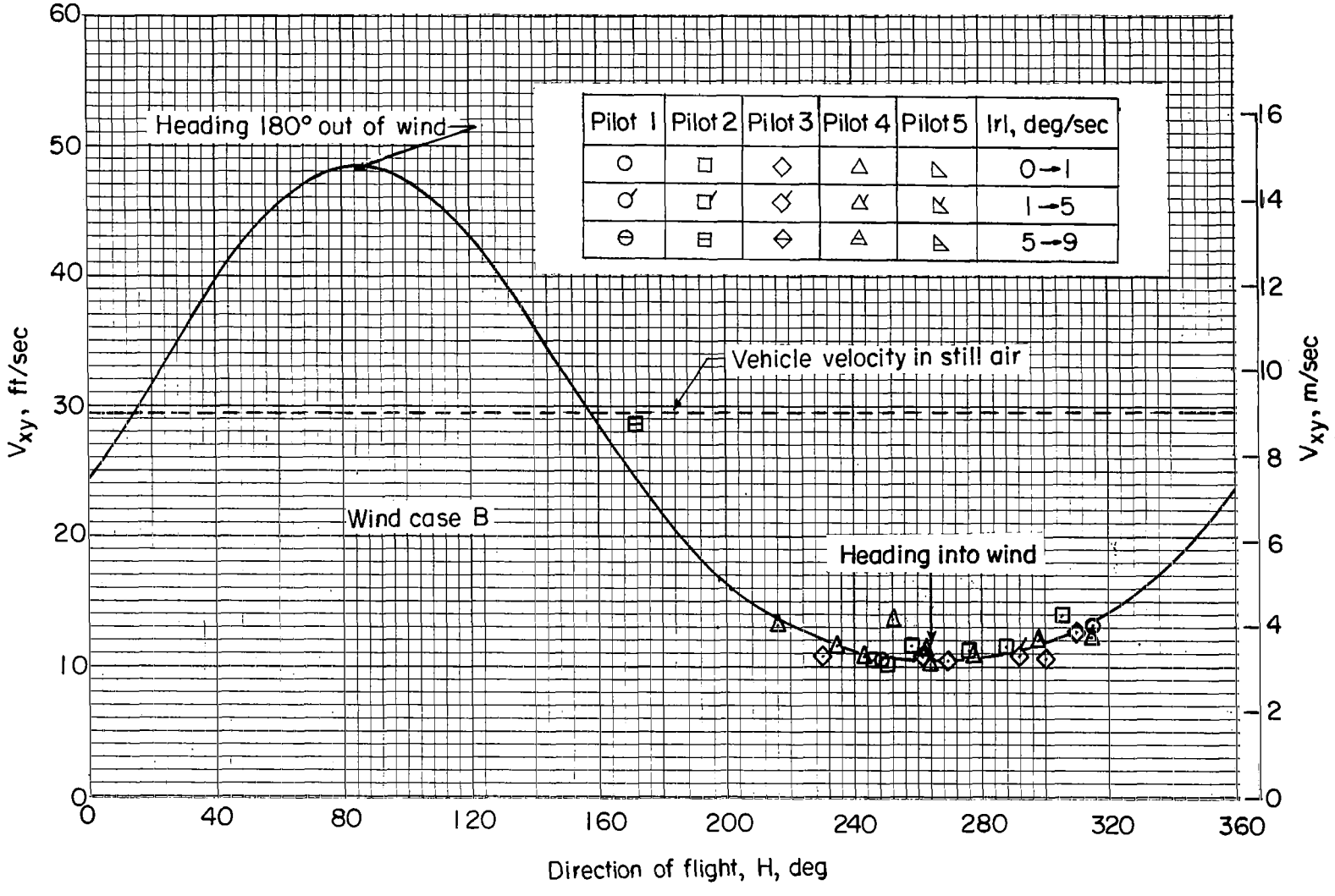

Figure 22.- Terminal ground speed, direction of flight, and turn rate for flights made in high winds.

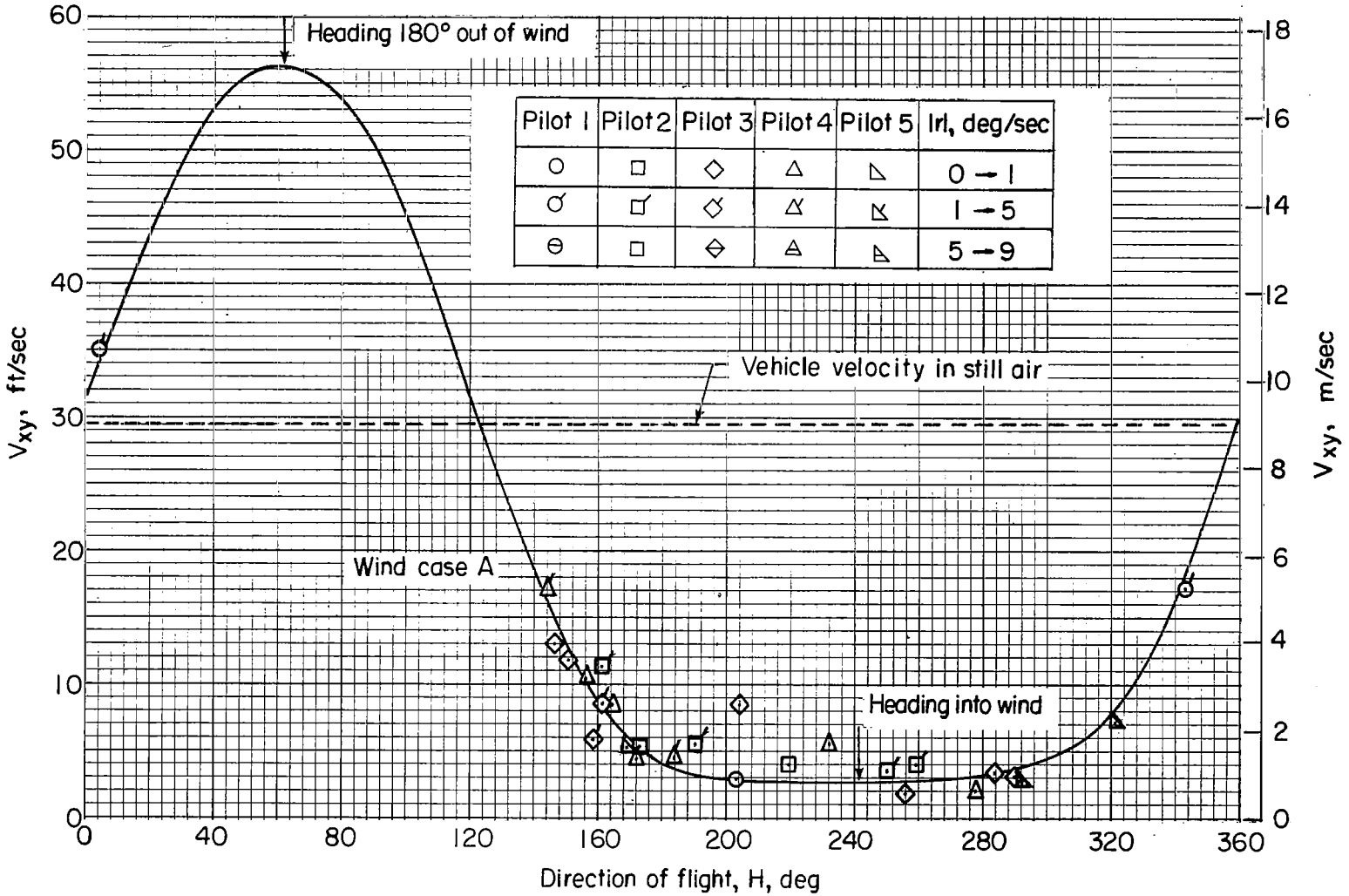

Figure 22.- Concluded.

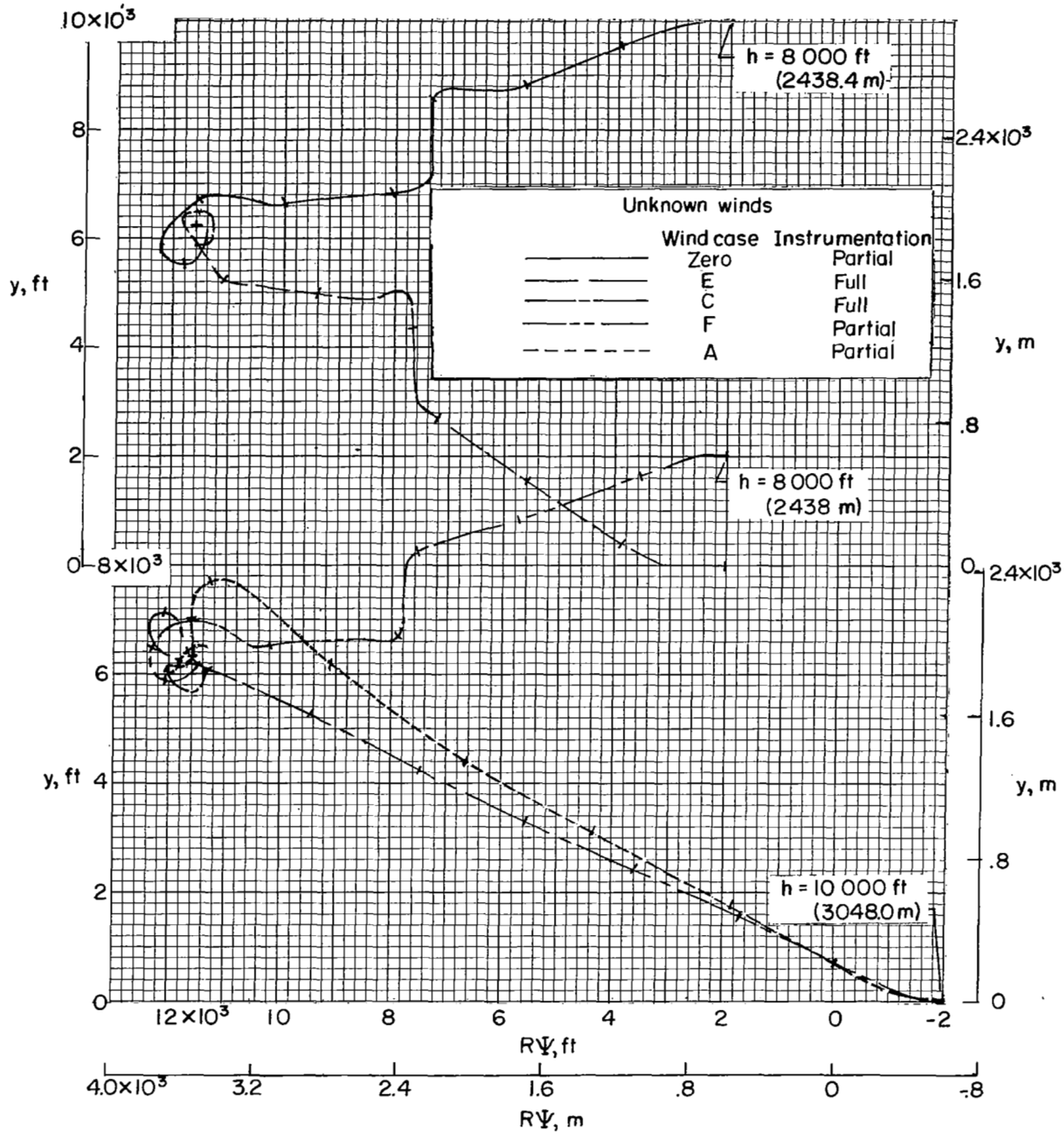

Figure 23.- Ground tracks of flights made under influence of unknown winds. (Tick marks indicate 1000-foot (304.8-meter) increments in altitude decreasing from the indicated initial value.)

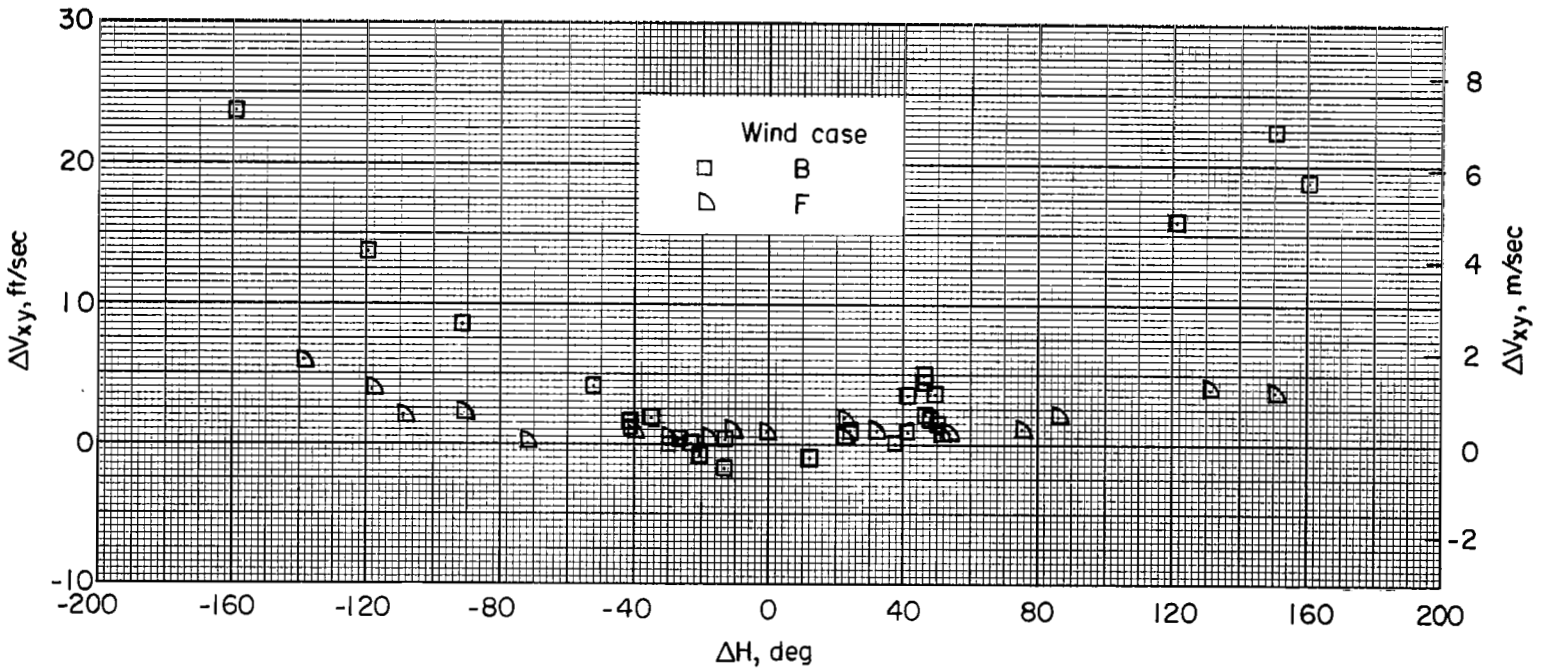

Figure 24.- Differences in terminal flight-path direction and ground speed from those which occur when headed into the wind for flights made under influence of unknown winds.